

1 **Volcanic ash modeling with the on-line NMMB/BSC-ASH-**
2 **v1.0 model: model description, case simulation and**
3 **evaluation**

4 **Alejandro Marti ^{(1)*}, Arnau Folch ⁽¹⁾, Oriol Jorba ⁽¹⁾ and Zavisla Janjic ⁽²⁾**

5 [1]{Barcelona Supercomputing Center (BSC-CNS), Barcelona, Spain}

6 [2]{National Center for Environmental Prediction, College Park, Maryland, USA}

7 (*) Correspondence to: Alejandro Marti (Alejandro.Marti@bsc.es)

8

9 **Abstract**

10 Traditionally, tephra transport and dispersal models have evolved decoupled (off-line) from numerical weather
11 prediction models. There is a concern that inconsistencies and shortcomings associated to this coupling strategy
12 might lead to errors in the ash cloud forecast. Despite this concern, and the significant progress to improve the
13 accuracy of tephra dispersal models in the aftermath of the 2010 Eyjafjallajökull and 2011 Cordón Caulle
14 eruptions, to date, no operational on-line dispersal model is available to forecast volcanic ash. Here, we describe
15 and evaluate NMMB/BSC-ASH, a new on-line multiscale meteorological and transport model that attempts to
16 pioneer the forecast of volcanic aerosols at operational level. The model [forecasts](#) volcanic ash cloud trajectories,
17 concentration of ash at relevant flight levels, and the expected deposit thickness for both regional and global
18 configurations. Its on-line coupling approach improves the current state-of-the-art of tephra dispersal models,
19 especially in situations where meteorological conditions are changing rapidly in time, two-way feedbacks are
20 significant, or distal ash cloud dispersal simulations are required. This work presents the model application for
21 the first phases of the 2011 Cordón Caulle and 2001 Mt. Etna eruptions. The computational efficiency of
22 NMMB/BSC-ASH and its application results compare favorably with other long-range tephra dispersal models,
23 supporting its operational implementation.

24

25 **Keywords:** volcanic ash, on-line coupling, transport-meteorological modeling, operational forecast, NWPM,
26 TTDM, Cordón Caulle, Mt. Etna.

27

28

29

30

Alex Marti 19/1/2017 15:41

Deleted: predicts

1 1 Introduction

2 Explosive volcanic eruptions can eject large quantities of particulate matter (tephra) that, along with other
3 aerosol droplets and trace gases, are carried upwards into the atmosphere by the buoyant eruption column and
4 then dispersed by winds aloft (e.g. Sparks et al., 1997). Tephra particles smaller than 2 mm in diameter,
5 technically defined as volcanic ash (Schmid, 1981), can spread over large distances away from the source
6 forming ash clouds that jeopardize air-traffic (Casadevall, 1993), airports (Guffanti et al., 2009) and, for very
7 large eruptions, alter both atmospheric composition and chemistry (Myhre et al., 2013; Self, 2006). Tephra
8 Transport and Dispersal Models (TTDMs, e.g. Folch, 2012) are used to simulate the atmospheric transport,
9 dispersion and ground deposition of tephra, and to generate operational short-term forecasts to support civil
10 aviation and emergency management. The recent eruptions of Eyjafjallajökull (Iceland) in 2010 and Cordón
11 Caulle (Chile) in 2011 have reinforced the importance of tephra dispersal in the context of global aviation safety.
12 In addition to short-term forecast, other model applications include the reconstruction of past events, studying
13 the impact of volcano eruptions on climate, probabilistic tephra hazard assessments or simulation of recent
14 eruptions for model evaluation purposes. For any of those cases, TTDMs require a driving Numerical Weather
15 Prediction Model (NWPM) or a meteorological reanalysis dataset for the description of the atmospheric
16 conditions, and an emission or source model for the characterization of the eruption column (Fig. 1).

17 Traditionally, TTDMs have evolved decoupled (off-line) from NWPMs. In the off-line strategy, the
18 meteorological driver runs *a priori* and independently of the TTDM to produce the required meteorological
19 fields at regular time intervals (e.g. hourly). Meteorological data is then furnished to the TTDM, which
20 commonly assumes constant values for the meteorological fields during each time interval or, at most, performs
21 a linear interpolation in time. Although the off-line approach is operationally advantageous, there is a concern
22 that it can lead to a number of accuracy issues (e.g. inaccurate handling of atmospheric processes) and
23 limitations (e.g. neglect of feedback effects) that can be corrected by on-line approaches (Grell et al., 2004).
24 These inconsistencies are especially important when meteorological conditions change rapidly in time or for
25 long-range transport. However, uncertainties arising from off-line systems have received little attention, even if
26 the experience from other communities (e.g. air quality) highlights the importance of coupling on-line dispersal
27 and meteorological models (e.g. Grell and Baklanov, 2011). To date, only the Weather Research and Forecasting
28 model with couple Chemistry (WRF-Chem; Grell et al., 2005) includes a coupled functionality that allows
29 simulating emission, transport, dispersion, transformation and sedimentation of pollutants released during
30 volcanic activities (Stuefer et al., 2013).

31 In this paper we describe and evaluate NMMB/BSC-ASH, a new on-line meteorological and atmospheric
32 transport model to simulate the emission, transport and deposition of ash (tephra) particles released from
33 volcanic eruptions. The model predicts ash cloud trajectories, concentration of ash at relevant flight levels, and
34 the expected deposit thickness for both regional and global domains. The novel on-line coupling in
35 NMMB/BSC-ASH allows solving both the meteorological and aerosol transport concurrently and interactively at
36 every time-step. This coupling strategy aims at improving the current state-of-the-art of tephra dispersal models,
37 especially in situations where meteorological conditions are changing rapidly in time, two-way feedbacks are
38 significant, or distal ash cloud dispersal simulations are required. The model builds on the NMMB/BSC
39 Chemical Transport Model (NMMB/BSC-CTM; Jorba et al., 2012; Pérez et al., 2011) to represent the transport

Alex Marti 19/1/2017 15:42

Deleted: slabs

Alex Marti 19/1/2017 15:48

Deleted: slab

1 of volcanic particles. Its meteorological core, the Non-hydrostatic Multiscale Model on a B grid (NMMB; Janjic
2 and Black, 2007; Janjic and Gall, 2012; Janjic, 2005; Janjic et al., 2011), allows for nested global-regional
3 atmospheric simulations by using consistent physics and dynamics formulations. The final objective in
4 developing NMMB/BSC-ASH is two-fold. On one hand, at a research level, we aim at studying the differences
5 between the on-line/off-line modeling strategies. Moreover, a second version of the model is projected to
6 quantify the feedback effects of dense volcanic ash clouds from large explosive eruptions on the radiative budget
7 and local meteorology. On the other hand, at an operational level, the low computational cost of the NMMB
8 dynamic core [presented in this work](#) suggests that NMMB/BSC-ASH could be applied for more accurate on-line
9 operational forecasting of volcanic ash clouds. Consequently, the focus on developing an on-line volcanic ash
10 model is timely.

11 This manuscript is arranged as follows: Section 2 summarizes the modeling background and the standard
12 physical schemes employed in NMMB/BSC-ASH; Section 3 provides a comprehensive description of the ash
13 related modules, including details about the emission, transport, and deposition of volcanic particles; Section 4
14 validates the regional and global configurations of the model with simulations for the 2001 Mt. Etna and 2011
15 Cordón Caulle long-lasting eruptions; Section 5 discusses the implementation [and performance](#) of the model for
16 its operational use and; finally, Section 6 provides a summary conclusion of this work.

17

18 **2 Modeling background**

19 NMMB/BSC-ASH is a novel on-line multi-scale meteorological and atmospheric transport model developed at
20 the Barcelona Supercomputing Center (BSC). The model attempts to pioneer the forecast of volcanic aerosols by
21 embedding a series of new modules on the BSC's operational system for short/mid-term chemical weather
22 forecasts (NMMB/BSC-CTM) developed at the BSC in collaboration with the U.S National Centers for
23 Environmental Prediction (NCEP) and the NASA Goddard Institute for Space Studies. The development of the
24 volcanic ash module follows the implementation of the mineral dust (Pérez et al., 2011) and sea-salt (Spada
25 et al., 2013) modules in NMMB/BSC-CTM, and allows for a range of different physical parameterizations for
26 research and operational use. The system allows for feedback processes among gases, aerosol particles and
27 radiation, and includes a gas-phase module to simulate tropospheric gas-phase chemistry (Badia et al., 2016;
28 Jorba et al., 2012).

29 Its meteorological core, the Non-hydrostatic Multiscale Model on the B grid (NMMB), is a fully compressible
30 meteorological model with a non-hydrostatic option that allows for nested global-regional atmospheric
31 simulations by using consistent physics and dynamics formulations. The standard physical and numerical
32 schemes employed in NMMB are summarized in Table 1. The non-hydrostatic dynamics were designed to avoid
33 over-specification. The cost of the extra non-hydrostatic dynamics is about 20% of the cost of the hydrostatic
34 part, both in terms of computer time and memory (Janjic, 2001, 2003). The numerical schemes for the
35 hydrostatic and nonhydrostatic options available in the NMMB dynamic solver were designed following the
36 principles found in Janjic (1977) and developed and modified thereafter (Janjic, 1979, 1984, 2003) and are
37 summarized in Janjic and Gall (2012). The Arakawa B-grid horizontal staggering is applied in the horizontal
38 coordinate employing a rotated latitude-longitude coordinate for regional domains and latitude-longitude

1 coordinate (Janjic, 2003) with polar filtering for global domains. Rotated latitude-longitude grids are employed
2 for regional simulations in order to obtain more uniform grid distances. In this particular case, the Equator of the
3 rotated system runs through the middle of the integration domain, reducing the longitudinal grid-size as the
4 southern and the northern boundaries of the integration domain are approached (Janjic and Gall, 2012). In the
5 vertical, the Lorenz staggering vertical grid is used with a hybrid sigma-pressure coordinate. The general time
6 integration philosophy in NMMB uses explicit schemes when possible for accuracy, computational efficiency
7 and coding transparency (e.g., horizontal advection), and implicit for very fast processes that would otherwise
8 require a restrictively short time-step for numerical stability with explicit differencing (e.g., vertical advection
9 and diffusion, vertically propagating sound waves). The NMMB model became the North American Mesoscale
10 (NAM) operational meteorological model in October of 2011, and it has been computationally robust, efficient
11 and reliable in operational applications and pre-operational tests since then. In high-resolution NWP
12 applications, the efficiency of the model significantly exceeds those of several established state-of-the-art non-
13 hydrostatic models (e.g. Janjic and Gall, 2012).

14

15 3 The volcanic ash module: BSC-ASH

16 The BSC-ASH module is embedded within the NMMB meteorological model and solves the mass balance
17 equation for volcanic ash taking into account: i) the characterization of the source term (emissions); ii) the
18 transport of volcanic particles (advection/diffusion); and iii) the particle removal mechanisms
19 (sedimentation/deposition). The coupling strategy of BSC-ASH can be turned on or off, depending on the
20 solution required (on-line vs. off-line). The on-line version of the model solves both the meteorological and
21 aerosol transport concurrently and consistently (on-line coupling). This strategy allows the particle transport to
22 be automatically tied to the model resolution time and space scales, resulting in a more realistic representation of
23 the meteorological conditions. In contrast, the off-line approach uses an “effective wind field” in which,
24 meteorological conditions (e.g. wind velocity, mid-layer pressure, etc.) are set to constant, and are only updated
25 at specific coupling intervals (i.e. time for which meteorological fluctuations are not explicitly resolved). This
26 strategy replicates the off-line coupling effect of traditional dispersal models used at operational levels (e.g.
27 coupling intervals of 1h or 6h). The conservativeness of the model is evaluated to ensure that the ash transport
28 scheme is consistent with the mass conservation equation.

29 3.1 Source term

30 Explosive volcanic eruptions release large amounts of particles into the atmosphere. These particles, commonly
31 known as tephra, mix with ambient air to form an eruption column or volcanic plume. To forecast the ash cloud
32 movement and provide actual ashfall concentrations, tephra dispersal models require a complete characterization
33 of the parameters describing the source term. These parameters are generally referred to as Eruption Source
34 Parameters (ESPs) and include the eruption start and duration, column height, mass eruption rate (MER), vertical
35 distribution of mass and the particle grain size distribution (GSD). ESPs vary not only from one eruption to
36 another, but also during the different eruptive phases of a single event.

Alex Marti 20/1/2017 13:43
Deleted: While t

Alex Marti 20/1/2017 13:44
Deleted: offers a more realistic representation

Alex Marti 20/1/2017 13:45
Deleted: ,

Alex Marti 20/1/2017 12:56
Deleted: s

Alex Marti 20/1/2017 13:50
Deleted: , which aims to replicate the decoupling effect of off-line dispersal models, for

Alex Marti 20/1/2017 14:06
Deleted: the wind velocity and mid-layer pressure (sigma) are set to constant during a given coupling interval.

1 Typically, the eruption starting time, duration and column height are inferred/constrained from visual or satellite
 2 observations. However, other parameters such GSD, MER, or the vertical distribution of mass in the column are
 3 not available in real-time and must be inferred from previous events of similar characteristics (e.g. Mastin et al.,
 4 2009). Uncertainties in source parameter values are a key factor limiting the accuracy of ash-cloud model
 5 forecasts (Bonadonna et al., 2015a). The characterization of each ESP in NMMB/BSC-ASH is described in the
 6 following subsections.

7 3.1.1 Mass eruption rate

8 The Mass Eruption Rate (MER) gives the mass released by unit of time and defines the eruption intensity. Its
 9 characterization in NMMB/BSC-ASH is achieved by employing a series of empirical correlations between
 10 (observed) column height and eruption rate, which, according to plume similarity theory, scales roughly as the
 11 4th power of height. Because of this strong dependence, uncertainties within 20% in the determination of column
 12 height can translate into uncertainties up to 70% for the MER (e.g., Biass and Bonadonna, 2011). Averaged
 13 column heights of eruptions that have not been directly observed are typically derived from characteristics of
 14 tephra deposits (e.g. Bonadonna and Costa, 2013; Carey and Sparks, 1986; Pyle, 1989), or derived from model
 15 inversion (e.g. Connor and Connor, 2006; Pfeiffer et al., 2005).

16 The empirical correlations to estimate MER in the model are described in Table 2, and are based either on fitting
 17 observations (e.g. Mastin et al., 2009), or more sophisticated fits accounting for wind bent-over effects (e.g.
 18 Degruyter and Bonadonna, 2012; Woodhouse et al., 2013). In addition, MER can also be derived using a more
 19 sophisticated 1-D plume model (see Sect. 3.1.5).

20 3.1.2 Vertical distribution of mass

21 The vertical distribution of mass in the column at the vent location is key when representing the plume,
 22 especially if wind shear exists with elevation at the volcano (Lin, 2012). To determine this distribution of mass,
 23 NMMB/BSC-ASH allows for the following geometrical distributions: i) point source, where mass is released as
 24 a single source point at a certain height above the vent, H_{plume} ; ii) top-hat, where mass is released along a
 25 umbrella-type slab of user-defined thickness, and iii) the so-called Suzuki distribution (Suzuki, 1983; Pfeiffer et
 26 al., 2005), which assumes a more complex vertical distribution of mass release along the eruption column;

$$S = MER \left\{ \left(1 - \frac{z}{H_{plume}} \right) \exp \left[A \left(\frac{z}{H_{plume}} - 1 \right) \right] \right\}^\lambda \quad (4)$$

28 where, S is the mass per unit of time (kg/s) released at a given height z above the vent, MER is the total mass
 29 eruption rate, H_{plume} is the column height above the vent, A and λ are the so-called Suzuki parameters. The
 30 parameter A dictates the height of the maximum particle release (concentration), whereas λ controls how closely
 31 mass distributes around this maximum. Any of the 3 options above can be combined independently with the
 32 different options for MER estimation. In NMMB/BSC-ASH, the terrain following hybrid sigma-pressure vertical

- Alex Marti 20/1/2017 14:53
Deleted: the initial
- Alex Marti 20/1/2017 14:54
Deleted:
- Alex Marti 20/1/2017 14:54
Deleted: shape
- Alex Marti 20/1/2017 14:55
Deleted: e
- Alex Marti 20/1/2017 14:55
Deleted: vertical
- Alex Marti 20/1/2017 14:55
Deleted: along the eruptive column
- Alex Marti 20/1/2017 15:02
Deleted:
- Alex Marti 31/1/2017 13:13
Deleted: (z)

1 levels of the model must be converted to elevations for each model integration time-step in order to interpolate
2 *MER* from the discrete source points into the nodes of the model grid.

3 3.1.3 Grain size distribution

4 The impact of explosive volcanic eruptions on climate and air traffic strongly depends on the concentration and
5 grain size distribution (GSD) of pyroclastic fragments injected into the atmosphere (e.g. Girault et al., 2014).
6 Grain size distribution is normally reconstructed by volcanologists from grain size data at individual outcrops,
7 ranging from basic unweighted average of the GSD at individual sparse outcrops, to various integration methods
8 of grain size data (e.g. Rose and Durant, 2009). The particle grain size distribution in NMMB/BSC-ASH is
9 specified through an input file, which defines the particle bin properties (bin mass fraction, diameter, density and
10 shape factor). In volcanology, grain size distributions are given in terms of the Φ , defined as $d = 2^{-\Phi}$, where d
11 is the particle diameter in mm. The granulometry file in the model can be furnished by the user (typically derived
12 from field data) or generated by an external utility program which produces Gaussian and Bi-Gaussian
13 distributions in Φ (log-normal in diameter d) (Costa et al., 2016; Folch et al., 2009).

14 3.1.4 Particle aggregation

15 The total grain size distribution (TGSD) erupted at the vent can be altered in case of particle aggregation, which
16 dramatically impacts particle transport dynamics thereby reducing the atmospheric residence time of aggregating
17 particles and promoting the premature fallout of fine ash. For computational purposes, particle aggregation in
18 NMMB/BSC-ASH is assumed to take place mainly in the eruption column, where particle concentration and
19 water contents are higher (the subsequent formation of aggregates downstream in the ash cloud under the
20 appropriate atmospheric conditions is not contemplated by the model). The model considers aggregates as
21 another particle class (bin), introduced as a standard source term by either solving: i) a series of simple analytical
22 expressions based on field observations or, ii) a more sophisticated wet aggregation model originally proposed
23 by Costa et al. (2010).

24 The analytical expressions available in the model modify the user-given particle grain size distribution by
25 assuming that a certain mass fraction of each granulometric class forms a new aggregate class added to the
26 TGSD. Despite the obvious limitations (obviates the physics of aggregation processes), these field-based
27 simplistic approaches are advantageous in that only the source term has to be modified in order to account for
28 aggregation. Table 3 provides an overview of these options. In addition to these empirical aggregation schemes,
29 NMMB/BSC-ASH also includes the wet aggregation model originally proposed by Costa et al. (2010). This
30 option allows for wet aggregation in the column providing an intermediate solution between the unaffordable all-
31 size class approach and the empirical solutions presented before. The model is based on a solution of the
32 classical Smoluchowski equation, obtained by introducing a similarity variable and a fractal relationship for the
33 number of primary particles in an aggregate. It also considers three different mechanisms for particle collision:
34 Brownian motion, ambient fluid shear, and differential sedimentation. Table 4 provides an overview of the
35 governing equations of this wet aggregation model.

Alex Marti 1/2/2017 19:21

Deleted: As typical in

Alex Marti 1/2/2017 19:20

Deleted: -number

1 3.1.5 FPlume model

2 A more sophisticated approach to obtain MER and the mass distribution in the column from the conditions at the
3 vent consists of solving a 1-D radially averaged BPT model for mass, momentum, and energy. These 1-D plume
4 models are more useful in operational roles and broad exploratory investigations (Costa et al., 2015; Devenish et
5 al., 2012). For that reason, NMMB/BSC-ASH is coupled with the 1-D FPlume model (Folch et al., 2015); a 1-D
6 cross-section averaged plume model which accounts for plume bent over, entrainment of ambient moisture,
7 effects of water phase changes on the energy budget, particle fallout and re-entrainment by turbulent eddies, as
8 well as variable entrainment coefficients fitted from experiments. The model also accounts for particle
9 aggregation in presence of liquid water or ice that depends on column dynamics, particle properties, and amount
10 of liquid water and ice existing in the column (Folch et al., 2010). This allows the plume model to predict an
11 “effective” grain size distribution depleted in fines with respect to that erupted at the vent. For a complete
12 definition of the governing equations of FPlume, refer to Folch et al. (2015). FPlume has two solving strategies
13 where the model: i) solves directly for column height for a given MER; or ii) solves iteratively for MER for a
14 given height. For any case, the following inputs need to be provided to the ash input file in NMMB/BSC-ASH:
15 eruption start and duration, vent coordinates and elevation, conditions at the vent (exit velocity, temperature,
16 magmatic water mass fraction, and total grain size distribution) and total column height or mass eruption rate.

17 3.2 Particle advection/diffusion

18 Transport of volcanic ash by advection and turbulent diffusion is analogous to those of atmospheric tracers (e.g.
19 moisture) transport (Janjic et al., 2009) in NMMB. Tracer advection is Eulerian, positive-definite and
20 monotonic. The Adams-Bashforth scheme is used for horizontal advection and the Crank-Nicolson scheme for
21 vertical advection. For the horizontal diffusion, the model uses a second order scheme with two types of
22 parameterized dissipative processes: explicit lateral diffusion (often called horizontal diffusion, a 2nd order
23 nonlinear Smagorinsky-type approach; Janjic, 1990) and horizontal divergence damping (Janjic and Gall, 2012).

24 Plumes from high-intensity eruptions can be injected high into the stratosphere, reaching a maximum column
25 height and intruding laterally at the neutral buoyancy level (NBL) as a gravity current (Sparks et al., 1997). This
26 current can spread at velocities exceeding those of the surrounding winds, affecting tephra transport and
27 deposition near the source. As larger particles are removed by deposition and air is entrained, the plume density
28 decreases and momentum reduces such that, at a certain distance, atmospheric turbulence and wind advection
29 become the dominant atmospheric transport mechanisms (Baines and Sparks, 2005). Neglecting the gravitational
30 spreading of the umbrella cloud in tephra dispersal simulations could misrepresent the interaction of the volcanic
31 ash cloud and the atmospheric wind field for high-intensity eruptions and for proximal deposition of tephra
32 (Mastin et al., 2014). To account for the gravity-driven transport, NMMB/BSC-ASH is coupled with the model
33 of Costa et al. (2013) describing cloud spreading as a gravity current. This parameterization calculates an
34 effective radial velocity of the umbrella spreading as a function of time or cloud radius. The effective radial
35 velocity of the umbrella spreading is then combined with the wind field velocity centered above the vent in the
36 umbrella region to calculate the contribution of the gravitational spreading to the total cloud spreading. To
37 estimate the radial distance at which the critical transition between gravity-driven and passive transport occurs,
38 the umbrella front velocity is compared with the mean wind velocity at the NBL estimating the Richardson

Alex Marti 20/1/2017 15:50

Deleted: h

1 number. Table 5 provides an overview of the governing equations of the gravity current model embedded in
2 NMMB/BSC-ASH.

3 3.3 Particle sedimentation and dry deposition

4 Particle sedimentation in NMMB/BSC-ASH is governed by the terminal velocity of settling particles. This fall
5 velocity is sensitive to particle size and atmospheric conditions, determining the residence time of ash particles
6 in the atmosphere. The NMMB/BSC-CTM model assumes that the settling velocities of aerosols (mineral dust,
7 sea salt, etc.) follow the Stokes law for spherical particles corrected by the Cunningham slip factor. The Stokes
8 law applies to the creeping or Stokes flow regime, in which the drag force is proportional to particle velocity,
9 and holds only for Reynolds numbers $Re \leq 0.1$. This regime is justified for small particles and aerosols ($< 20 \mu\text{m}$).
10 However, calculating fallout times based on settling according to Stokes Law is less adequate for coarse ash ($>$
11 $64 \mu\text{m}$), which sediments much faster. In addition, ash particles are not spherical, which complicates and further
12 slows fallout. In order to simulate properly a wider spectrum of particle sizes, NMMB/BSC-ASH adds a new
13 sedimentation module that covers the turbulent regime ($Re \geq 1000$) in which, the drag force is proportional to the
14 square of the particle velocity. In this case, the gravitational particle settling velocity, v_s (in $m \cdot s^{-1}$), can be
15 expressed as:

16

$$v_s = \sqrt{\frac{4g(\rho_p - \rho_a)d}{3C_d\rho_a}} \quad (13)$$

17 where, ρ_a and ρ_p denote air and particle density, respectively, d is the particle equivalent diameter, and C_d is the
18 drag coefficient (depending on the Reynolds number). Strictly, the expression above is valid for spherical
19 particles in the turbulent regime but it is often generalized to the whole range of Re numbers and particle shapes
20 by defining the drag coefficient properly. Table 6 provides an overview of the different settling velocity models
21 available in NMMB/BSC-ASH, each relying on different empirical evaluations of drag coefficient.

22 Dry deposition, acting at the bottom layer of the model, is a complex process depending on physical and
23 chemical properties of the particle, the underlying surface characteristics and micro-meteorological conditions.
24 Dry deposition in NMMB/BSC-ASH is based on that originally proposed by Zhang et al. (2001). This
25 parameterization has been updated to account for the different settling velocities available for volcanic particles -
26 Eq. (13). The dry deposition velocity in the model, v_d (in $m \cdot s^{-1}$), is given by:

27

$$v_d = v_s + \frac{1}{(R_a - R_s)} \quad (18)$$

Alex Marti 6/2/2017 13:43

Deleted: sedimenting

Alex Marti 6/2/2017 13:44

Deleted: method is considered an efficient removal mechanism

Alex Marti 6/2/2017 13:45

Deleted: . Therefore, calculated

Alex Marti 6/2/2017 13:45

Deleted: are inaccurate

Alex Marti 6/2/2017 13:46

Deleted: where

Alex Marti 20/1/2017 16:03

Deleted: a

1 where, R_a is the aerodynamic resistance of the particle, and R_s is the surface resistance (both in $s \cdot m^{-1}$). These
2 terms take into account all the effects of the lowermost layer of the atmosphere, such as turbulence (R_a) and
3 Brownian diffusion, impaction and interception (R_s). It is worth mentioning that, for most of its resident time,
4 airborne volcanic ash lies above the near-surface atmospheric layers, where gravitation dominates, implying that,
5 in most cases, dry deposition has little influence on model results.

6 3.4 Mass conservation

7 Mass conservation is a critical requirement for any atmospheric transport algorithm. Non-conservative schemes
8 can significantly underestimate or overestimate concentrations, especially for long time integrations, in which it
9 is critical that the tracer advection scheme is consistent with the mass continuity equation (Jöckel et al., 2001).
10 Most mesoscale meteorological models use observation/analyzed fields or global model results as initial
11 conditions, and therefore they are not very sensitive to slowly accumulated mass inconsistencies as re-
12 initializations remove accumulations. However, dispersal models are usually very sensitive to mass
13 inconsistencies set in previous simulations or spin-up fields as initial conditions, thereby accumulating mass
14 inconsistencies. In addition to mass conservation, monotonicity and prevention of non-physical under and
15 overshoots in the solution are also a highly desirable characteristics in transport schemes (Rood, 1987). For these
16 reasons, the model includes a conservative, positive definite (i.e. tracer is a positive scalar) and monotone (i.e.
17 entirely increasing) Eulerian scheme for advection. The positive definiteness in the model is guaranteed by
18 advecting the square root of the tracer using a modified Adams-Bashforth scheme for the horizontal direction
19 and a Crank-Nicolson scheme for the vertical direction. The conservation of the tracer is achieved as a result of
20 the conservation of quadratic quantities by the advection scheme. Monotonization is applied *a posteriori* to
21 eliminate new extrema (Janjic et al., 2009). The conservative nature of NMMB/BSC-ASH is evaluated by
22 calculating the mass flux at the boundaries (for regional domains) of the computational domain, the airborne
23 mass, and the mass deposited on the ground to verify mass conservation at each time-step (e.g. < 0.5% mass
24 creation for a 30 day simulation).

25 3.5 Numerical performance

26 The high computational efficiency of the NMMB meteorological driver allows for the application of
27 nonhydrostatic dynamics at a global scale (Janjic et al., 2009), and supports that the NMMB/BSC-ASH could be
28 used in an operational forecast of volcanic ash clouds. Model parallelization is based on the well-established
29 Message Passing Interface (MPI) library. The computational domain is decomposed into sub-domains of nearly
30 equal size in order to balance the computational load, where each processor is in charge to solve the model
31 equations in one sub-domain. The Eulerian schemes in the model require relatively narrow and constant width
32 halos (i.e. data points from the computational domain of neighboring sub-domains that are replicated locally for
33 computational convenience), which simplify and reduce communications.

34 To measure the time-to-solution required, we compute the parallel speed-up (computation speed) of the model;
35 that is, the performance gains of parallel processing in comparison to serial processing:

36

Alex Marti 20/1/2017 16:52

Deleted: Nicholson

$$S_{(P)} = \frac{t_{(P=1)}}{t_{(P)}} \quad (19)$$

where S is the computed speed-up value, and t is the simulation run-time employing P processors instead of running it serially ($P = 1$).

To evaluate the efficiency of the model while using the computational resources, the parallel efficiency of the model is computed by looking at the ratio between the parallel speed-up over P :

$$E_{(P)} = \frac{S_{(P)}}{P} \quad (20)$$

Parallel efficiency is used as a metric to determine how far the model's speed-up is from the ideal. If the speed-up is ideal, the efficiency is 1, regardless of how many cores the program is running on. If the speed-up is less than ideal, the efficiency is less than 1.

4 Simulations and validation

The forecast skills of NMMB/BSC-ASH have been tested for several well-characterized eruptions, including the Pinatubo 1991 (Philippines), Etna 2001 (Italy), Chaitén 2008 (Chile) or Cordon Caulle 2011 (Chile) eruptions (e.g. Marti et al., 2013, 2014). Here, we present two applications of the model for the ash dispersal forecast of weak and strong long lasting eruptions. Section 4.1 summarizes the results of the regional and global simulations for the first days of the 2011 Cordón Caulle eruption. This event represents a suitable case study of strong long-lasting eruptions with changing winds, which is useful to evaluate the advantages of the on-line approach for operational forecast. In a parallel effort, Sect. 4.2 summarizes the results from the regional configuration of the model for the 2001 Etna eruption. This eruption is a good example of a weak, long-lasting eruption, useful when evaluating the sedimentation mechanisms of the model against well-characterized tephra deposits.

4.1 The 2011 Cordón Caulle eruption

The 2011 Cordón Caulle eruption was a typical mid-latitude Central and South Andean eruption, where dominating winds carried ash clouds over the Andes causing abundant ash fallout across the Argentine Patagonia. Besides the significant regional impacts on agriculture, livestock and water distribution systems, this eruption stranded thousands of passengers due to air traffic disruptions in the southern hemisphere, thereby causing important economic losses to airlines and society (e.g. Raga et al., 2013; Wilson et al., 2013). This event is evidence of the global nature of the volcanic ash dispersion phenomena and highlights the need for accurate real-time forecasts of ash clouds.

The Cordón Caulle volcanic complex (Chile, 40.5° S, 72.2° W, vent height 1420 m a.s.l.) reawakened on 4 June 2011 around 18:30 UTC after decades of quiescence. The initial explosive phase spanned more than two weeks,

Alex Marti 1/2/2017 20:12

Deleted: .

Alex Marti 26/1/2017 16:30

Deleted: when evaluating the

Alex Marti 26/1/2017 16:30

Deleted:

Alex Marti 26/1/2017 16:35

Deleted: coupling

Alex Marti 26/1/2017 16:31

Deleted: strategy

Alex Marti 26/1/2017 16:31

Deleted: of the model

Alex Marti 26/1/2017 16:39

Deleted: .

Alex Marti 20/1/2017 17:19

Deleted: s

Alex Marti 20/1/2017 17:20

Deleted: over

1 | generating ash clouds that dispersed over the Andes. The climactic phase (~27 h) (Jay et al., 2014) was
2 | associated with a ~9 km (a.s.l.) high column (Osores et al., 2014). For the period between 4 - 14 June, numerous
3 | flights were disrupted in Paraguay, Uruguay, Chile, southern Argentina and Brazil. The two major airports
4 | serving Buenos Aires and the international airport in Montevideo, Uruguay, were closed for several days, along
5 | with airports in Patagonia (Wilson et al., 2013). A detailed chronology of the eruption can be found in Collini et
6 | al. (2013) and (Elissondo et al., 2016), the stratigraphy and characteristics of the resulting fallout deposit are
7 | described in Pistolesi et al. (2015) and Bonadonna et al., (2015b), and a summary of the environmental impacts
8 | of the eruption is discussed in Raga et al. (2013) and Wilson et al. (2013).

9 | Here, we describe the synoptic meteorological situation during the first two weeks of eruptive activity (Fig. 2),
10 | and give a brief chronology of the events in order to compare them with the predictions of the model. The
11 | eruption developed as a long-lasting rhyolitic activity with plume heights above the vent between around 9-10
12 | km high a.s.l. (4-6 June), 4 and 9 km during the following week (7-14 June) and < 6 km after 14 June (Global
13 | Volcanism Program, GVP, <http://www.volcano.si.edu>; Siebert et al. 2010). The first major episode, on 4 June
14 | (18:45 UTC), resulted in an ash cloud (9-10 km) that reached the Chile-Argentina border within the hour of the
15 | eruption. On June 5, E-SE winds drove the plume to the Atlantic Ocean (1800 away from the source), leaving a
16 | large area of Argentina territory affected by ash fall. On June 6, the plume changed its direction abruptly toward
17 | N-NE, reaching the northern regions of the Argentine Patagonia, and then shifted direction again towards SE,
18 | threatening the Buenos Aires air space. On June 7, a second episode resulted in a plume (4-9 km) dispersing ash
19 | further to the north of Argentina leading to a more recognizable shift of winds over the E-SE. On June 8, the
20 | volcanic cloud (9-10 km a.s.l.) dispersed towards NE with a bend toward SE 400 km from the source. On June 9,
21 | the plume had a NE direction reaching the city of Buenos Aires and the northern boundary of Paraguay
22 | following a frontal zone passing through Patagonia. This resulted in major air traffic disruption at the two
23 | international airports that service the city: Aeroparque (AEP) and Ezeiza (EZE), which remained closed
24 | intermittently during the following 15 days. Later during the day, the wind turned SE dispersing ash over
25 | Uruguay, Brazil and Paraguay. Ash cloud continued to change in direction over the next 6 days, with clouds
26 | following the ridge structure to the NE and SE, respectively.

27 | 4.1.1. Regional simulation

28 | *Model set-up*

29 | The model domain for the regional run is presented in Table 7 and consists of 268x268 grid points covering the
30 | northern regions of Chile and Argentina using a rotated latitude-longitude grid with a horizontal resolution of
31 | 0.15° x 0.15° and 60 vertical layers. The top pressure of the model was set to 21 hPa (~34 km) with a mesh
32 | refinement near the top (to capture the dispersion of ash) and the ground (to capture the characteristics of the
33 | atmospheric boundary layer). The computational domain spans in longitude from 41° W to 81° W and in latitude
34 | from 18° S to 58° S. Runs were performed with the on-line version of NMMB/BSC-ASH from 3 June 2011 at
35 | 00:00 UTC to 21 June 2011 at 00:00 UTC. The integration time-step for the meteorological core and aerosol
36 | transport was set to 30 seconds. The dynamic time-steps for the long and short wave radiations were computed
37 | every 120 time-steps. Feedback effects of ash particles on meteorology and radiation were not included in this

Alex Marti 26/1/2017 12:26

Moved down [1]: Figure 2 shows the synoptic meteorological situation during the 6-16 June.

Alex Marti 26/1/2017 12:26

Moved (insertion) [1]

Alex Marti 26/1/2017 13:47

Deleted: we give a brief chronology of the events Figure 2 shows

Alex Marti 26/1/2017 14:03

Deleted: the synoptic meteorological situation during the 6-16 June, that occurred

Alex Marti 26/1/2017 13:47

Deleted:

Alex Marti 26/1/2017 13:43

Deleted: In particular, we focus on the three major dispersion episodes occurring between the 6 - 8 June. The first major episode, on 6 June, resulted in a cloud moving northwards at high atmospheric pressure (300 hPa), reaching the northern regions of the Argentine Patagonia threatening the Buenos Aires air space. This resulted in major air traffic disruption at the two international airports that service the city: Aeroparque (AEP) and Ezeiza (EZE), which remained closed intermittently during the following 15 days. A complementary episode dispersed ash further to the north of Argentina leading to a more recognizable shift of winds over the E-SE. In the morning of 7 June, the initial trough reached the northern boundary of Paraguay coinciding with fallout of snow and rain over Patagonia. Later during the day, the wind turned SE dispersing ash over Uruguay, Brazil and Paraguay. During 8 and 9 June, the trough intensified, shifting the ash dispersion NE throughout the trough-ridge structure. During the first hours of 9 June, the ash cloud reached the city of Buenos Aires following a frontal zone passing through Patagonia, leaving a thin ash layer across the area.

Alex Marti 26/1/2017 13:06

Formatted: Not Highlight

Alex Marti 26/1/2017 13:53

Deleted: Afterwards, the cloud travelled S-SE, affecting the southern part of the Patagonia and Chile.

1 run. The meteorological driver was initialized with wind fields from the Era-Interim reanalysis at $0.75^\circ \times 0.75^\circ$
2 resolution as initial and 6-h boundary conditions. In order to reduce the errors in meteorological conditions, they
3 were reinitialized every 24 h with a spin-up of 12 h. Daily eruption source parameters (ESP) were obtained from
4 Osores et al. (2014), who estimated column heights for each eruptive pulse using the Imager Sensor data from
5 the GOES-13 satellite, [applying the cloud-top IR image technique](#) (Kidder and VonderHaar, 1995). Mass flow
6 rate released along the column was derived from column heights based on Mastin et al. (2009), assuming a
7 Suzuki vertical distribution of mass typical of explosive Plinian eruptions ($A=4$; $\lambda=5$). Grain size distribution
8 was obtained from Collini et al. (2013) and discretized in 10 bins ranging from -1Φ (2 mm) to 8Φ (4 μm) with a
9 linear dependency of particle density on diameter ranging from 1.000 to 2.200 kg m^{-3} . Particle sphericity was set
10 to a constant standard value of 0.9 for all bins. The *percentage* aggregation model was used to update the TGSD
11 with a new bin for aggregates, resulting in a total of 11 bins.

12 *Validation of results against satellite imagery*

13 Model results for the airborne mass concentration of ash were validated using qualitative and quantitative
14 comparisons with data obtained using two different techniques. On one end, we performed a qualitative
15 comparison between the simulated column mass (g m^{-2}) from the model and the NOAA-AVHRR satellite
16 imagery provided by the high-resolution picture transmission (HRPT) division of the Argentinian National
17 Meteorological Service. Figure 3 shows how the NMMB/BSC-ASH predictions for cloud trajectory and arrival
18 times are in agreement with observations, capturing the three major dispersion episodes. It should be noted that
19 these types of images are not directly comparable because the MODIS ash detection threshold and the
20 reflectivity coefficients of volcanic ash are not well constrained. However, the figure illustrates the capability of
21 the model to predict the variation of the cloud position with time.

22 Column mass simulations were also validated against ash mass loadings presented by (Osores et al., 2015), who
23 retrieved ash-contaminated pixels detected on the basis of the concept of reverse absorption (Prata, 1989a,
24 1989b), i.e. those pixels with brightness temperature differences between 11 and 12 μm (BTD11-12 μm) that are
25 lower than 0.0 K. To minimize the presence of false positives, pixels with a BTD11-12 $\mu\text{m} > -0.6$ K and clear
26 sky pixels were removed. Mass loadings were mapped up to 15 g m^{-2} based on an approach which combines the
27 satellite data with look-up tables of brightness temperatures obtained with a radiative transfer model and optical
28 properties of andesite volcanic rocks (Prata, 2011). Figure 4 shows a good quantitative agreement between the
29 model results and the airborne ash mass loadings described above.

30 *Validation of results against fallout deposit*

31 Tephra was mostly deposited eastward from the source during the first 72 h of the event within an elongated area
32 between $40\text{-}42^\circ$ S and $64\text{-}72^\circ$ W. Results from the NMMB/BSC-ASH forecast for ash deposition were validated
33 against: i) a detailed characterization of the proximal deposit for the first 72 h of the eruption, and ii) an isopach
34 map derived from measurements taken for the period beginning on 4 June until 30 June (Collini et al., 2013).

35 To evaluate the simulated computed thicknesses (cm) by the model near the vent during the first 72 h of the
36 event, model results were compared against a comprehensive classification of the proximal deposit presented by
37 Pistolesi et al. (2015b), who constrained the stratigraphic sequence of the deposit in different Units (phases).

1 Here, we constrain the deposit to the first three units of their work, corresponding to the first 72 h of the eruptive
2 even and including: i) Unit I, containing coarser-grained layers A-B, representing the very first stage of the
3 eruption within the first 50 km from the vent, and layers A–F associated to the first 24–30 h of the eruption
4 (afternoon of 4 to morning of 5 June); ii) Unit II, containing layer H, a fine pumice lapilli layer which was
5 emplaced starting on the night of 6 June; iii) Unit III, enclosing layer K2, the easiest to identify from several
6 coarser (fine-lapilli) grain-size layers, and being associated to the morning of 7 June. Figure 5 shows that
7 NMMB/BSC-ASH can reproduce the deposit presented by Pistolesi et al. (2015b) both in time and space. Key
8 sections located along the dispersal area (e.g. San Carlos de Bariloche – SCB, 90 km from the vent; Ingeniero
9 Jacobacci – IJ, 240 km east of the vent) were used as geographic references.

10 To evaluate the model performance at the end of our simulation, model results were also validated against an
11 isopach map derived from measurements taken from the 4 to 30 June presented by Collini et al. (2013). Deposit
12 load variations produced by remobilization were not considered in this analysis. Figure 6 shows good agreement
13 between the modeled deposit load (kg m^{-2}) at the end of the simulation and the measured ground deposit
14 isopachs (kg m^{-2}) at 30 June from Collini et al. (2013).

15 The model resulted in a cumulative mass of $\sim 4.2 \times 10^{11}$ kg. This value is in agreement with previous works,
16 where total mass was either modeled (Collini et al., 2013) or estimated by empirical fits (Bonadonna et al.,
17 2015b). Ashfall forecast with the NMMB/BSC-ASH model represented well the overall deposit load for the
18 2011 Caille eruption.

19 4.1.2 Global simulation

20 For this simulation, the global domain was configured using a regular latitude–longitude grid with a horizontal
21 resolution of $0.75^\circ \times 1^\circ$ and 60 vertical layers. The ash distribution is simulated between 3–21 June 2011 using
22 the Era-Interim reanalysis at $0.75^\circ \times 0.75^\circ$ resolution as initial and 6-h boundary conditions. Meteorological
23 conditions for the global runs were also [reinitialized](#) every 24h. The atmospheric model’s fundamental time-step
24 was set to 180 s, while the rest of the model variables [and grain size distribution](#) remained the same as in the
25 regional simulation. Figure 7 shows the global dispersal of ash for the 2011 Cordon Caille eruption after
26 different times of the simulation. As it can be inferred from this figure, by 10 June, the plume entered
27 the Australian and New Zealand airspace (Fig 7b) covering more than half of the southern hemisphere. At that
28 point, the Civil Aviation Authority of New Zealand warned pilots that the ash cloud was between 20,000 and
29 35,000 feet (6 to 11 kilometers), the average cruising level for many aircraft (Sommer, 2011). Before the end of
30 our simulation, on 13 June the ash cloud had completed its first circle around the globe. This is in agreement to
31 satellite images reported by the Darwin Volcanic Ash Advisory Centre (Darwin VAAC, 2011). Finally, results
32 from the global simulation are also in agreement with those from our regional run.

33 4.1.3 Forecasting impacts on civil aviation

34 NMMB/BSC-ASH can furnish values of airborne concentration at relevant flight levels (FL), defined as the
35 vertical altitude (expressed in hundred of feet) at standard pressure at which the ash concentration is measured.
36 This information is particularly important for air traffic management and can be used to decide alternative routes
37 to avoid an encounter with a volcanic cloud. Airborne concentration at FL050 (5,000 feet on nominal pressure) is

Alex Marti 27/1/2017 10:52

Deleted: reinitialized

Alex Marti 26/1/2017 18:22

Deleted:

1 | relevant for the determination of flight cancellations and airports closures, while concentrations at FL300
2 | (30,000 feet) are critical to assist flight dispatchers while planning flight paths and designing alternative routes in
3 | the presence of a volcanic eruption. The model runs as if responding to an eruptive event, i.e. we only used the
4 | semi-quantitative data available at that time as volcanological inputs.

5 | Figure 8 shows the airspace contamination forecasted by NMMB/BSC-ASH during the 6-7 June at flight levels
6 | FL050 and FL300, within a latitude band between 20° S and 55° S. Model results show the volcanic cloud
7 | twisting in different directions during that period of time, achieving critical concentration values within a wide
8 | area east of the Andes range. On 6 June, simulation results show the volcanic cloud at high atmospheric pressure
9 | (~ 30,000 feet or 300 hPa) moving northwards, and the one at lower atmospheric pressure (~ 5,000 ft or 50 hPa)
10 | threatening the main international airports that service the region of Buenos Aires (Fig. 8a). In the morning of 7
11 | June, the ash cloud present at lower atmospheric pressure (~ 5,000 ft or 50 hPa) changed its direction towards the
12 | SW, ultimately affecting part of the Patagonia and Chile (Fig. 8b), while higher ash clouds started their course
13 | around the globe (Fig. 8c). These results suggest that the cancellation of multiple flights in several Argentinean
14 | airports during this time was justified. It is important to point out that, for this work, our objective is not to
15 | perform a detailed study of the Caulle eruption but to use it as a blind test to confront short-term model
16 | predictions and semi-quantitative syn-eruptive observations.

17 | 4.2 The 2001 Mt. Etna eruption

18 | Mt. Etna is the most active volcano in Europe and constitutes a continuous hazard for eastern Sicily. Since 1980,
19 | Mt. Etna has injected large volumes of pyroclasts into the atmosphere (between 10^4 and 10^7 m³ per event) over
20 | more than 160 eruptive episodes (Scollo et al., 2012). The explosive activity of Mt. Etna reached its climax in
21 | 2001 and 2002–03 when two major flank eruptions occurred; both characterized by long-lasting explosive
22 | activity (Branca and Del Carlo, 2005). The 2001 event represents a good case to evaluate the deposition
23 | mechanisms of NMMB/BSC-ASH against the well-characterized tephra deposit reported in Scollo et al. (2007).
24 | The explosive activity at the 2570 m vent had three main phases characterized by phreatomagmatic, magmatic
25 | and vulcanian explosions. The eruption started with a series of phreatomagmatic explosions during the first days
26 | of the eruption. These explosions were followed by a second eruptive phase characterized by strombolian and
27 | Hawaiian style explosions during 19-24 July. The explosive activity continued until 6 August with a series of
28 | vulcanian explosions. Tephra fallout associated to the explosive activity during 21-24 July represented a major
29 | source of hazard for eastern Sicily. Flight operations were cancelled at the Catania and Reggio Calabria airports
30 | during the 22 and 23 July (Scollo et al., 2007). A detailed chronology of the eruption can be found in Scollo et
31 | al. (2007). Volcanic plumes were captured by the Multiangle Imaging Spectro Radiometer (MISR) on board
32 | NASA's Terra spacecraft, and analyzed with stereo matching techniques to evaluate the height of the volcanic
33 | aerosol with a precision of a few hundred meters (Scollo et al., 2012).

34 | Here, we validate NMMB/BSC-ASH against the tephra deposit produced from the 2570 m vent for that period of
35 | time, and compare the model performance against simulations results from the FALL3D model (Costa et al.,
36 | 2006; Folch et al., 2009) for the same event. FALL3D is an Eulerian model for transport and deposition of
37 | volcanic ash particles solving a set of advection-diffusion-sedimentation equations (one equation for each
38 | particle class) on a structured terrain, following grid using a second-order Finite Differences explicit scheme. The

1 | [FALL3D](#) model is used at the Buenos Aires and Darwin Volcanic Ash Advisory Centers (VAAC) in operational
2 forecasts.

3 **4.2.1 Regional simulation**

4 ***Model set-up***

5 Two regional domains were used to simulate the first phase of the 2001 eruption of Mt. Etna (Table 8). The first
6 domain (Regional 1), used to reconstruct the tephra deposit, consists of 101x101 grid points covering the SE
7 flank using a rotated latitude–longitude grid with a horizontal resolution of 0.05° x 0.05° and 60 vertical layers.
8 Similarly to the Cordón Caulle simulations, the top pressure of the model was set to 21 hPa (~34 km) with a
9 mesh refinement near the top and ground. The computational domain spans in longitude from 12.5° E to 17.5° E,
10 in latitude from 35.25° N to 40.25° N. Simulation runs were performed with the on-line version of NMMB/BSC-
11 ASH from 21 July 2001 at 00:00 UTC to 25 July 2001 at 00:00 UTC. The integration time-step for the
12 meteorological core was set to 10 seconds. The meteorological driver was initialized with Era-Interim reanalysis
13 meteorological data at 0.75° x 0.75° resolution as initial and 6-h boundary conditions. A spin-up of 12 h was used
14 to prepare the meteorological conditions for run. Each daily model run was reinitialized with the corresponding
15 reanalysis, the NMMB/BSC-ASH tracers' output from the previous day, and the associated eruption source
16 parameters. Meteorological conditions were reinitialized every 24 h. The grain size distribution and eruption
17 source parameters were obtained from Scollo et al. (2007), who assumed a Suzuki vertical mass distribution
18 located at the middle of the eruption column ($A=2$; $\lambda=1$), and employed the Mastin et al. (2009) empirical
19 relationship to characterize the MER and the Voronoi tessellation method to obtain the grain size distribution.
20 Finally, sensitivity analyses were performed against the different aggregation schemes available in the model. In
21 all cases, the TGSD was updated with a new bin for aggregates, resulting in a total of 8 bins.

22 A second regional domain (Regional 2) was used to evaluate tephra dispersal between 21 and 25 of July. In this
23 case, the domain consisted of 201x201 grid points covering a computational domain spanning in longitude from
24 41° E to 81° E, in latitude from 18° S to 58° S. This domain used a coarser horizontal resolution of 0.1° x 0.1° and
25 60 vertical layers. The integration time-step for the meteorological core was set to 30 seconds. The rest of model
26 set-up was kept the same as in the first regional domain (Regional 1).

27 ***Validation of results against fallout deposit***

28 At the end of the second explosive phase, a continuous tephra layer covered Etna's flanks between Giarre and
29 Catania (from E to S). Ash deposition results from NMMB/BSC-ASH were validated against 47 samples
30 collected between 25 and 26 July from measured areas on flat open spaces, where the deposit did not show any
31 reworking. The computed tephra dispersal and deposition from NMMB/ABSC-ASH was able to reproduce the
32 bilobate shape of the real deposit with the two axes oriented toward Acireale and Acicastello towns. Figure 9
33 compares the simulated deposit load (kg m^{-2}) at the end of the run against the isopachs map derived from
34 measurements taken from the 21-24 July (Scollo et al., 2007). The model resulted in a cumulative mass of
35 | $\sim 1.18 \times 10^9$ kg. This value is in agreement with the results obtained from Scollo et al. (2007).

4.2.2 Model intercomparison: NMMB/BSC-ASH vs. FALL3D

To validate the model performance of NMMB/BSC-ASH for its operational implementation, we compare the tephra deposition results of the model against those of the operational FALL3D model for the reconstruction of the 2001 Mt. Etna eruption. For this comparison we ran both models using the same meteorological and volcanological initial conditions (Table 8). Figure 10 shows the simulated thicknesses (vertical axis) for both transport models against the observations (horizontal axis) presented in Scollo et al. (2007). The model improved the tephra distribution results from FALL3D simulations for the same event (R^2 ; 0.80/0.62), reducing the RMSE (0.014/0.24) and bias (0.02/0.6) and the computational time by an order of magnitude. In particular, all values simulated with NMMB/BSC-ASH plot inside the region between 5 and 1/5 (dashed orange line) times the observed mass at each station. The greatest differences observed against the observations for both models belong to those points located at distances less than 15 km from the vent associated to the uncertainty in the ESPs. The mean value of the relative error between the computed values and observed data is 64%, which improves those from FALL3d (91%), and are comparable with those of Scollo et al., (2007), who obtained a 57% by deposit best-fitting using the HAZMAP dispersion model

5 Operational forecast with NMMB/BSC-ASH

The Barcelona Supercomputing Center is currently working on a modeling integrated system to provide operational forecast of volcanic ash with NMMB/BSC-ASH. The system includes a preprocessing tool (prepares the model for real-data simulations), an executable file to run the model, and a user-based postprocessing utility tool. Figure 11 shows a simple schematic representation of the operational implementation of NMMB/BSC-ASH. The outcomes of this modeling system are currently being evaluated against two operational models: i) the NOAA/ARL Hybrid Single Particle Lagrangian Integrated Trajectory Model (HYSPPLIT; Draxler and Hess, 1998) – used at the Washington VACC; and FALL3D (Costa et al., 2006; Folch et al., 2009) – used at the Buenos Aires and Darwin VAACs. This section introduces the structure of the operational NMMB/BSC-ASH system. Preliminary results for the model intercomparison against FALL3D are described in Sect. 4.2.2.

5.2 The preprocessing system

The preprocessing utility system consists of a set of programs whose collective role is to prepare the model for real-data simulations. Programs are grouped to preprocess geographical, meteorological and climatological inputs and interpolate them to the model grid(s). The preprocessing system uses three main programs: *runfix*, *degrib* and *runvariable*.

- *Runfix* defines the model domain(s) and interpolates static geographical data to the model grid(s). In addition to computing the latitude and longitude of the rotated grid points, this program interpolates soil categories, land use types, terrain height, annual mean deep soil temperature, monthly albedo, maximum snow albedo, and slope category.
- *Degrib* extracts the necessary meteorological fields from GRIB-formatted files, used as initial condition for global simulations and as initial and boundary conditions for single regional domains (i.e. not nested

Alex Marti 31/1/2017 22:03

Deleted: Employing on-line models for operational dispersal forecast requires larger computational resources and is not always feasible at all operational institutes. Nevertheless, due to the increase in computing power of modern systems, one can argue that such gradual migration towards stronger on-line coupling of NWP models with TDMS poses a challenging but attractive perspective from the scientific point of view for the sake of both high-quality meteorological and volcanic ash forecasting. The focus on volcanic aerosols integrated systems in operational forecast is timely, since recent research has shown that meteorology and chemistry feedbacks are important in the context of many research areas and applications (e.g., NWP and air quality forecasting, climate and Earth system modeling). -

... [1]

1 with a global domain). GRIB files contain time-varying meteorological fields obtained from another
2 regional or global NWPM. In addition to the available NCEP's North American Model (NAM) or
3 Global Forecast System (GFS) model, the program has been updated to include European Centre for
4 Medium-Range Weather Forecasts (ECMWF) ERA-Interim reanalysis data (Dee et al., 2011) as
5 forcing.

- 6 • *Runvariable* interpolates the meteorological fields extracted by *debgrib* to the model grid(s) defined by
7 *runfix* and prepares the climatological schemes. This program generates the initial and boundary
8 conditions that are ingested by NMMB using the NOAA Environmental Modeling System (NEMS;
9 Janjic, 2005; Janjic and Black, 2007), a high performance software superstructure and infrastructure
10 based on the Earth System Modeling Framework (ESMF) for use in operational prediction models at
11 NCEP.

12 5.3 BSC-ASH I/O files

13 The model takes three run-specific input files:

- 14 • The model input file (*nmmmb.inp*), which defines the computational and physical schemes needed by the
15 meteorological core, the atmospheric model's fundamental time-step, and the parameterization for
16 chemical processes and radiative schemes for aerosol tracers (including ash), amongst other properties
17 of the model. For long-lasting eruptions, the model performs restart runs initializing the tracers from the
18 previous day's history file.
- 19 • The ash input file (*ash.inp*), [which defines those parameters employed in the ash module](#). The user-
20 defined parameters include: [i\) the characterization of the source term](#): eruption source type, column
21 height and determination of the mass eruption rate, eruption duration, [aggregation processes](#), and
22 particle settling velocity model. In the event of various eruptive phases, the respective ESPs for each
23 phase can be defined; [ii\) the settings to turn on/off the gravity current model altering the particle](#)
24 [transport in the umbrella cloud](#); and [iii\) the definition of the coupling strategy \(on vs. off-line\)](#)
25 employed by the model.
- 26 • The granulometry input file (*ash.tgsd*), which specifies the diameter, density, sphericity, and relative
27 mass fraction of each particle bin. This information is typically obtained from field data or created by
28 external utility programs for idealized grain size distributions. If aggregation is active, a new bin class
29 for aggregates is added to the granulometry input file.

30 Once a simulation is concluded, NMMB/BSC-ASH writes the following output files:

- 31 • A log file (*ash.log*), containing information about the run, including a summary of the computed
32 volcanic ash source and mass balance statistics for each time-step, and errors and warnings if any.
- 33 • A forecast results file (*problemname.nc*) in NetCDF format containing, amongst other variables, the
34 total column mass concentration (g m^{-2}) and ground deposition (kg m^{-2}) for all bins, the concentration at
35 different Flight Levels (g m^{-3}) and the Aerosol Optical Depth. This information can be processed using
36 several open-source programs to generate plots and animations. Alternatively, the post-process utility
37 program *NMMB2GMT* has been developed to generate basic GMT scripts automatically.

Alex Marti 27/1/2017 13:13

Deleted: which defines the source term

Alex Marti 27/1/2017 13:24

Deleted:

Alex Marti 27/1/2017 13:01

Deleted: gravity current conditions,

Alex Marti 27/1/2017 13:24

Deleted: . Finally, the file also

Alex Marti 27/1/2017 13:03

Deleted: defines t

- A restart file (*nmmh.hst*) used to initiate a new run using the ash concentrations from a previous simulation.

5.4 The Postprocess system

The postprocess utility tools are designed to interpolate outputs from the NMMB/BSC-ASH native grid(s) to National Weather Service (NWS) standard levels (pressure, height, etc.) and standard output grids (Lambert Conformal, polar-stereographic, etc.) in NetCDF format. The system also includes the *NMMB2GMT* program, which uses the Generic Mapping Tools (GMT) software (Wessel and Smith, 1991) to produce similar plots to the Volcanic Ash Graphics (VAG) used by Volcanic Ash Advisory Centers in operational forecasts.

5.5 Scalability analysis

To optimize a future operational implementation of the model, we aim to minimize the time-to-solution avoiding communication overhead. In this context, we evaluate the model scalability (scaling efficiency) for its regional and global configurations by performing a strong scalability test, in which the problem size of our simulation (e.g., model domain and resolution) remains fixed while increasing the number of processing cores. Figure 12 shows the parallel speed-up (S ; Eq. 19), and efficiency (E ; Eq. 19) of the NMMB/BSC-ASH system for a global simulation of the climatic phase for the 2011 Cordón Caulle (Table 7). On the MareNostrum-III supercomputer, maximum efficiency for the global simulation described in Table 7 is reached between 32-40 nodes (16 CPUs each) with a parallel efficiency of 0.6.

The scalability analysis was performed on all the available source term and sedimentation schemes in the model. The relative computational cost associated with the main processes in NMMB/BSC-ASH is presented in Fig. 13. Processes represented include: meteorological prediction, volcanic ash transport and sedimentation forecast, aggregation of particles, gravity current effects, and the restart phase. The restart phase represents the CPU time employed to rerun the preprocess system every 24h of simulation. This figure suggests that the computational increase (CPU time) associated to the ash module can vary from 5 to 55%, depending on the number of computational nodes employed. It is important to note that, depending on the settling velocity model employed, up to 60% of the time allocated to the ash module is assigned to the sedimentation term.

Results from the scalability analysis show that the model performance (in terms of speed-up) depends on the problem size as well as on the domain partitioning topology. In that context, the relative computational cost of the model's meteorological core (NMMB) is evaluated as a function of its domain decomposition (e.g., distribution of processing units for the horizontal domains – nodes i and j). For this analysis the bin-performance dependency of the model is considered, therefore evaluating only the cost of one bin of ash. Results from this analysis suggest that, for an optimal simulation using 32 nodes, the computational cost of the meteorological core decreases over 10 % when the weight of the decomposition is focused on the j nodes (e.g., more computational resources assigned for the Fast Fourier Transformation algorithm). The best domain decomposition resulted in $6(i) \times 84(j) + 8(w)$, where i and j , are the number of processors employed in the horizontal and vertical domains respectively, and w , the number of writing processors.

Alex Marti 27/1/2017 13:28

Deleted: at ≈

Alex Marti 27/1/2017 13:28

Deleted:

Alex Marti 27/1/2017 13:33

Deleted: ,

Alex Marti 27/1/2017 13:33

Formatted: Font:Italic

Alex Marti 27/1/2017 13:32

Deleted: being t

1 For operational purposes, the computational time employed to provide ash dispersal forecast using NMMB/BSC-
2 ASH is evaluated for the global simulation with 1 bin of ash. The maximum time required by the model to
3 perform a 24 h forecast, running all the available processes (e.g., advection, diffusion, sedimentation, etc.) every
4 time-step (180 seconds) is less than 3 minutes when using the best domain decomposition presented before
5 (6x84+8). This time can be further optimized for operational purposes, i.e., calling the model physics less
6 frequently in order to save computational time. As a general rule of thumb, the adjustment time-step in seconds
7 for the meteorological core can be taken as 2.25 times the grid spacing in kilometers. For higher resolution
8 model runs made without parameterized convection, a time-step in seconds of about 1.9 to 2.0 times the grid
9 spacing may be more appropriate (Janjic and Gall, 2012).

10 5.6 Cost-benefit analysis

11 Employing on-line models for operational dispersal forecast requires larger computational resources and is not
12 always feasible at all operational institutes. Nevertheless, due to the increase in computing power of modern
13 systems, one can argue that such gradual migration towards stronger on-line coupling of NWPMs with TDMs
14 poses a challenging but attractive perspective from the scientific point of view for the sake of both high-quality
15 meteorological and volcanic ash forecasting.

16 The focus on volcanic aerosols integrated systems in operational forecast is timely. Experiences from other
17 communities (e.g. air quality) have shown the benefits from two-way online meteorology-chemistry modeling.
18 For example, the importance of the different feedback mechanisms for meteorological and atmospheric
19 composition processes have been previously discussed for models developed in the USA (Zhang, 2008) and
20 Europe (Baklanov et al., 2014). These benefits have been recently stressed by several studies covering the
21 analysis of the aerosol-transport and aerosol-radiation feedbacks onto meteorology from the air quality model
22 evaluation international initiative (AQMEII) in its phase 2 (Alapaty et al., 2012; Galmarini et al., 2015) and the
23 EuMetChem COST Action ES1004 (EuMetChem, <http://eumetchem.info>).

24 Demonstrating these benefits however, require running the on-line model with and without feedbacks over
25 extended periods of time. For the particular case of volcanic aerosols, further research is still required to quantify
26 the benefits posed by on-line couple models over traditional off-line TTDM on both atmospheric transport and
27 the radiative budget. The Barcelona Supercomputing Center is currently working to quantify these benefits with
28 NMMB/BSC-ASH model, and assess how the magnitude of the model forecast errors implicit in the off-line
29 approach compares with other better-constrained sources of forecast error, e.g. uncertainties in eruption source
30 parameters. Preliminary results from this study indicate that meteorology-transport inconsistencies from off-line
31 models can be, in some cases, in the same order of magnitude that those associated to the eruption source
32 parameters. In terms of computational cost, the computational efficiency of the NMMB/BSC-ASH
33 meteorological core allows for on-line integrated operational forecasts employing an equivalent computational
34 time than FALL3D for the same computational domain and number of processing cores.

Alex Marti 1/2/2017 11:21

Formatted: Font color: Black

1 **6 Summary and Conclusions**

2 We present NMMB/BSC-ASH, a new on-line multiscale meteorological and transport model developed at the
3 Barcelona Supercomputing Center (BSC) to forecast the dispersal and deposition of volcanic aerosols. The
4 objective of NMMB/BSC-ASH is to improve the current state-of-the-art of tephra dispersal models, especially in
5 situations where meteorological conditions are fluctuating rapidly in time, two-way feedbacks are significant, or
6 long-range ash cloud dispersal predictions are necessary. The model predicts ash cloud trajectories,
7 concentration of ash at relevant flight levels, and the expected deposit thickness for both regional and global
8 domains. NMMB/BSC-ASH solves the mass balance equation for volcanic ash by means of a new ash module
9 embedded in the BSC's operational system for short/mid-term chemical weather forecasts (NMMB/BSC-CTM).
10 In addition to volcanic ash, the system is also capable to forecast the dispersion of other atmospheric aerosols
11 (e.g. dust, sea salt, black carbon, organic aerosol, sulfates, etc.). Its multiscale capability allows for nested
12 global-regional atmospheric transport simulations, taking into account the characterization of the source term
13 (emissions), the transport of volcanic particles (advection/diffusion), and the particle removal mechanisms
14 (sedimentation/deposition). The model has been shown to be robust and scalable to arbitrary domain sizes
15 (regional to global) and numbers of processors.

16 The forecast skills of NMMB/BSC-ASH have been validated against several well-characterized eruptions,
17 including the, Etna 2001 (Italy), Chaitén 2008 (Chile), Cordón Caulle 2011 (Chile) or Pinatubo 1991
18 (Philippines) eruptions (e.g. Marti et al., 2013, 2014). To evaluate the on-line coupling strategy and the
19 multiscale capability of the model, this paper summarizes the regional and global configurations of the model to
20 forecast the dispersal of ash for the first days of the 2011 Cordón Caulle eruption (strong long-lasting eruption
21 with rapid wind changes). In addition, to evaluate the sedimentation mechanisms of the model, this work also
22 includes the results from the regional configuration of the model for the first phase of the 2001 Etna eruption, a
23 good case study of weak long-lasting eruption with well-characterized tephra deposits. Simulation results
24 demonstrate that NMMB/BSC-ASH is capable to reproduce the spatial and temporal dispersal variability of the
25 ash cloud and tephra deposits.

26

27 **Software**

28 The work described in this paper is based on version 2.0.1 (released in April, 2014). The code, written in
29 FORTRAN-90, is portable and efficient on available parallel computing platforms. The figures presented in this
30 paper were generated using Gnuplot and NCAR Command Language (NCL).

31

32 **Acknowledgements**

33 The research leading to these results has received funding from the People Programme (Marie Curie Actions) of
34 the European Union's Seventh Framework Programme (FP7/2007-2013) under the project NEMOH (REA grant
35 agreement n° 289976). O. Jorba partially funded by grant CGL2013-46736 of the Ministry of Economy and
36 Competitiveness of Spain. We are extremely grateful to the Argentinian National Meteorological Service for
37 sharing data to validate this work; in particular we thank M.S. Osoreo for providing valuable insights into the

1 eruption dynamics. Numerical simulations were performed at the Barcelona Supercomputing Center with the
2 MareNostrum Supercomputer using 512 and 256 - 8x4 GB DDR3-1600 DIMMS (2GB/core) Intel SandyBridge
3 processors, iDataPlex Compute Racks, a Linux Operating System and an Infiniband interconnection.

4

5 **Competing interests**

6 The authors declare that they have no conflict of interest.

7

1 **References**

- 2 Alapaty, K., Herwehe, J. A., Otte, T. L., Nolte, C. G., Bullock, O. R., Mallard, M. S., Kain, J. S. and Dudhia, J.:
3 Introducing subgrid-scale cloud feedbacks to radiation for regional meteorological and climate modeling,
4 *Geophys. Res. Lett.*, 39(24), 1–5, doi:10.1029/2012GL054031, 2012.
- 5 Ames, W.: *Numerical methods for partial differential equations*, Nelson. London., 1969.
- 6 Arastoopour, H., Wang, C.-H. and Weil, S. A.: Particle-particle interaction force in a dilute gas-solid system,
7 *Chem. Eng. Sci.*, 37(9), 1379–1386, doi:10.1016/0009-2509(82)85010-0, 1982.
- 8 Badia, A., Jorba, O., Voulgarakis, A., Dabdub, D., Pérez García-Pando, C., Hilboll, A., Gonçalves, M. and
9 Janjic, Z.: Gas-phase chemistry in the online multiscale NMMB/BSC Chemical Transport Model: Description
10 and evaluation at global scale, *Geosci. Model Dev. Discuss.*, (2), 1–47, doi:10.5194/gmd-2016-141, 2016.
- 11 Baines, P. and Sparks, R. S. J.: Dynamics of giant volcanic ash clouds from supervolcanic eruptions, *Geophys.*
12 *Res. Lett.*, 32(December), 1–4, doi:10.1029/2005GL024597, 2005.
- 13 Baklanov, A., Schlünzen, K., Suppan, P., Baldasano, J. M., Brunner, D., Aksoyoglu, S., Carmichael, G., Douros,
14 J., Flemming, J., Forkel, R., Galmarini, S., Gauss, M., Grell, G., Hirtl, M., Joffre, S., Jorba, O., Kaas, E., Kaasik,
15 M., Kallos, G., Kong, X., Korsholm, U., Kurganskiy, A., Kushta, J., Lohmann, U., Mahura, A., Manders-Groot,
16 A., Maurizi, A., Moussiopoulos, N., Rao, S. T., Savage, N., Seigneur, C., Sokhi, R. S., Solazzo, E., Solomos, S.,
17 Sørensen, B., Tsegas, G., Vignati, E., Vogel, B. and Zhang, Y.: Online coupled regional meteorology chemistry
18 models in Europe: Current status and prospects, *Atmos. Chem. Phys.*, 14(November 2013), 317–398,
19 doi:10.5194/acp-14-317-2014, 2014.
- 20 Betts, A. K. and Miller, M. J.: A new convective adjustment scheme. Part II: Single column tests using GATE
21 wave, BOMEX, ATEX and arctic air-mass data sets, *Q. J. R. Meteorol. Soc.*, 112(473), 693–709,
22 doi:10.1002/qj.49711247308, 1986.
- 23 Biass, S. and Bonadonna, C.: A quantitative uncertainty assessment of eruptive parameters derived from tephra
24 deposits: The example of two large eruptions of Cotopaxi volcano, Ecuador, *Bull. Volcanol.*, 73(1), 73–90,
25 doi:10.1007/s00445-010-0404-5, 2011.
- 26 Bonadonna, C. and Costa, A.: Plume height, volume, and classification of explosive volcanic eruptions based on
27 the Weibull function, *Bull. Volcanol.*, 75, 1–19, doi:10.1007/s00445-013-0742-1, 2013.
- 28 Bonadonna, C., Biass, S. and Costa, A.: Physical characterization of explosive volcanic eruptions based on
29 tephra deposits: Propagation of uncertainties and sensitivity analysis, *J. Volcanol. Geotherm. Res.*,
30 doi:10.1016/j.jvolgeores.2015.03.009, 2015a.
- 31 Bonadonna, C., Cioni, R. and Pistolesi, M.: Sedimentation of long-lasting wind-affected volcanic plumes : the
32 example of the 2011 rhyolitic Cordón Caulle eruption, Chile, *Bull. Volcanol.*, doi:10.1007/s00445-015-0900-8,
33 2015b.
- 34 Branca, S. and Del Carlo, P.: Types of eruptions of Etna volcano AD 1670-2003: Implications for short-term
35 eruptive behaviour, *Bull. Volcanol.*, 67(8), 732–742, doi:10.1007/s00445-005-0412-z, 2005.

- 1 Carey, S. and Sparks, R. S. J.: Quantitative models of the fallout and dispersal of tephra from volcanic eruption
2 columns, *Bull. Volcanol.*, 48(2–3), 109–125, doi:10.1007/BF01046546, 1986.
- 3 Casadevall, T. J.: *Volcanic Hazards and Aviation Safety : Lessons of the Past Decade.*, 1993.
- 4 Collini, E., Osores, M. S., Folch, A., Viramonte, J., Villarosa, G. and Salmuni, G.: Volcanic ash forecast during
5 the June 2011 Cordón Caulle eruption, *Nat. Hazards*, 66, 389–412, doi:10.1007/s11069-012-0492-y, 2013.
- 6 Connor, L. and Connor, C.: *Inversion is the Key to Dispersion : Understanding Eruption Dynamics by Inverting*
7 *Tephra Fallout*, Special Publications of IAVCEI, 1. Geological Society, London, pp. 231–242., 2006.
- 8 Cornell, W., Carey, S. and Sigurdsson, H.: Computer simulation of transport and deposition of the Campanian
9 Y-5 ash, *J. Volcanol. Geotherm. Res.*, 17, 89–109, 1983.
- 10 Costa, A., Macedonio, G. and Folch, A.: A three-dimensional Eulerian model for transport and deposition of
11 volcanic ashes, *Earth Planet. Sci. Lett.*, 241, 634–647, doi:10.1016/j.epsl.2005.11.019, 2006.
- 12 Costa, A., Folch, A. and MacEdonio, G.: A model for wet aggregation of ash particles in volcanic plumes and
13 clouds: 1. Theoretical formulation, *J. Geophys. Res. Solid Earth*, 115, 1–14, doi:10.1029/2009JB007175, 2010.
- 14 Costa, A., Folch, A. and Macedonio, G.: Density-driven transport in the umbrella region of volcanic clouds :
15 Implications for tephra dispersion models, *Geophys. Res. Lett.*, 40(July), 4823–4827, doi:10.1002/grl.50942,
16 2013.
- 17 Costa, A., Suzuki, Y., Cerminara, M., Devenish, B. J., Esposti Ongaro, T., Herzog, M., Van Eaton, A., Denby,
18 L., Bursik, M., De’ Michieli Vitturi, M., Engwell, S., Neri, A., Barsotti, S., Folch, A., Macedonio, G., Girault, F.,
19 Carazzo, G., Tait, S., Kaminski, É., Mastin, L., Woodhouse, M., Phillips, J., Hogg, A., Degruyter, W. and
20 Bonadonna, C.: Overview of the Results of the Eruption Column Model Intercomparison Exercise, *J. Volcanol.*
21 *Geotherm. Res.*, doi:10.1016/j.jvolgeores.2016.01.017, 2015.
- 22 Costa, A., Pioli, L. and Bonadonna, C.: Assessing tephra total grain-size distribution: Insights from field data
23 analysis, *Earth Planet. Sci. Lett.*, 443(September), 90–107, doi:10.1016/j.epsl.2016.02.040, 2016.
- 24 Darwin VAAC: Satellite image of path of the Cordon Caulle ash cloud around the southern hemisphere from 5-
25 12 June 2011, *Bur. Meteorol.* [online] Available from: http://www.bom.gov.au/info/vaac/cordon_caulle.shtml,
26 2011.
- 27 Dee, D. P., Uppala, S. M., Simmons, a. J., Berrisford, P., Poli, P., Kobayashi, S., Andrae, U., Balmaseda, M. a.,
28 Balsamo, G., Bauer, P., Bechtold, P., Beljaars, a. C. M., van de Berg, L., Bidlot, J., Bormann, N., Delsol, C.,
29 Dragani, R., Fuentes, M., Geer, a. J., Haimberger, L., Healy, S. B., Hersbach, H., Hólm, E. V., Isaksen, L.,
30 Kållberg, P., Köhler, M., Matricardi, M., McNally, a. P., Monge-Sanz, B. M., Morcrette, J. J., Park, B. K.,
31 Peubey, C., de Rosnay, P., Tavolato, C., Thépaut, J. N. and Vitart, F.: The ERA-Interim reanalysis:
32 Configuration and performance of the data assimilation system, *Q. J. R. Meteorol. Soc.*, 137(April), 553–597,
33 doi:10.1002/qj.828, 2011.
- 34 Degruyter, W. and Bonadonna, C.: Improving on mass flow rate estimates of volcanic eruptions, *Geophys. Res.*
35 *Lett.*, 39(May), 1–6, doi:10.1029/2012GL052566, 2012.

- 1 Dellino, P., Mele, D., Bonasia, R., Braia, G., La Volpe, L. and Sulpizio, R.: The analysis of the influence of
2 pumice shape on its terminal velocity, *Geophys. Res. Lett.*, 32(October), 1–4, doi:10.1029/2005GL023954,
3 2005.
- 4 Devenish, B. J., Francis, P. N., Johnson, B. T., Sparks, R. S. J. and Thomson, D. J.: Sensitivity analysis of
5 dispersion modeling of volcanic ash from Eyjafjallajökull in May 2010, *J. Geophys. Res. Atmos.*, 117(D20), n/a-
6 n/a, doi:10.1029/2011JD016782, 2012.
- 7 Draxler, R. R. and Hess, G. D.: An Overview of the HYSPLIT_4 Modelling System for Trajectories, Dispersion,
8 and Deposition., *Aust. Meteorol. Mag.*, 47(June 1997), 295–308, 1998.
- 9 Elissondo, M., Baumann, V., Bonadonna, C., Pistolesi, M., Cioni, R., Bertagnini, A., Biass, S., Herrero, J. C. and
10 Gonzalez, R.: Chronology and impact of the 2011 Cordon Caulle eruption, Chile, *Nat. Hazards Earth Syst. Sci.*,
11 16(3), 675–704, doi:10.5194/nhess-16-675-2016, 2016.
- 12 Ferrier, B., Jin, Y., Lin, Y., Black, T., Rogers, E. and DiMego, G.: Implementation of a new grid-scale cloud and
13 precipitation scheme in the NCEP Eta Model, in *Proc. 15th Conf. on Numerical Weather Prediction*; San
14 Antonio; 12–16 August 2002; TX, pp. 280–283, American Meteorological Society., 2002.
- 15 Folch, A.: A review of tephra transport and dispersal models: Evolution, current status, and future perspectives,
16 *J. Volcanol. Geotherm. Res.*, 235–236, 96–115, doi:10.1016/j.jvolgeores.2012.05.020, 2012.
- 17 Folch, A., Costa, A. and Macedonio, G.: FALL3D: A computational model for transport and deposition of
18 volcanic ash, *Comput. Geosci.*, 35, 1334–1342, doi:10.1016/j.cageo.2008.08.008, 2009.
- 19 Folch, A., Costa, A. and Macedonio, G.: A model for wet aggregation of ash particles in volcanic plumes and
20 clouds: 1. Theoretical formulation, *J. Geophys. Res. Solid Earth*, 115, 1–16, doi:10.1029/2009JB007175, 2010.
- 21 Folch, A., Costa, A. and Macedonio, G.: FPLUME-1.0: An integrated volcanic plume model accounting for ash
22 aggregation, *Geosci. Model Dev. Discuss.*, 8(9), 8009–8062, doi:10.5194/gmdd-8-8009-2015, 2015.
- 23 Gadd, A.: An economical explicit integration scheme. Tech. Note 44. UK Meteorological Office., 1974.
- 24 Galmarini, S., Hogrefe, C., Brunner, D., Baklanov, A. and Makar, P.: Preface Article for the Atmospheric
25 Environment Special Issue on AQMEII Phase 2, *Atmos. Environ.*, (115), 340–344, 2015.
- 26 Ganser, G. H.: A rational approach to drag prediction of spherical and nonspherical particles, *Powder Technol.*,
27 77(2), 143–152, doi:http://dx.doi.org/10.1016/0032-5910(93)80051-B, 1993.
- 28 Girault, F., Carazzo, G., Tait, S., Ferrucci, F. and Kaminski, É.: The effect of total grain-size distribution on the
29 dynamics of turbulent volcanic plumes, *Earth Planet. Sci. Lett.*, 394, 124–134, doi:10.1016/j.epsl.2014.03.021,
30 2014.
- 31 Grell, G. and Baklanov, A.: Integrated modeling for forecasting weather and air quality: A call for fully coupled
32 approaches, *Atmos. Environ.*, 45(38), 6845–6851, doi:10.1016/j.atmosenv.2011.01.017, 2011.
- 33 Grell, G. a., Knoche, R., Peckham, S. E. and McKeen, S. a.: Online versus offline air quality modeling on cloud-
34 resolving scales, *Geophys. Res. Lett.*, 31(April), 6–9, doi:10.1029/2004GL020175, 2004.

1 Grell, G. a., Peckham, S. E., Schmitz, R., McKeen, S. a., Frost, G., Skamarock, W. and Eder, B.: Fully coupled
2 “online” chemistry within the WRF model, *Atmos. Environ.*, 39, 6957–6975,
3 doi:10.1016/j.atmosenv.2005.04.027, 2005.

4 Guffanti, M., Mayberry, G. C., Casadevall, T. and Wunderman, R.: Volcanic hazards to airports, *Nat. Hazards*,
5 51(2), 287–302, doi:10.1007/s11069-008-9254-2, 2009.

6 Janjic, Z.: Pressure gradient force and advection scheme used for forecasting with steep and small scale
7 topography, *Beiträge zur Phys. der Atmosphäre*, 50(1), 186–199, 1977.

8 Janjic, Z.: Forward-backward scheme modified to prevent two-grid-interval noise and its application in sigma
9 coordinate models, *Contrib. Atmos. Phys.*, 52, 69–84, 1979.

10 Janjic, Z.: Nonlinear Advection Schemes and Energy Cascade on Semi-Staggered Grids, *Mon. Weather Rev.*,
11 112, 1234–1245, doi:10.1175/1520-0493(1984)112<1234:NASAEC>2.0.CO;2, 1984.

12 Janjic, Z.: The Step-Mountain Coordinate: Physical Package, *Mon. Weather Rev.*, 118(7), 1429–1443,
13 doi:10.1175/1520-0493(1990)118<1429:TSMCPP>2.0.CO;2, 1990.

14 Janjic, Z.: The Step-Mountain Eta Coordinate Model: Further Developments of the Convection, Viscous
15 Sublayer, and Turbulence Closure Schemes, *Mon. Weather Rev.*, 122(5), 927–945, doi:10.1175/1520-
16 0493(1994)122<0927:TSMECM>2.0.CO;2, 1994.

17 Janjic, Z.: The Mellor-Yamada level 2.5 turbulence closure scheme in the NCEP Eta Model, *WORLD Meteorol.*
18 *Organ. TD*, 4–14, 1996.

19 Janjic, Z.: Nonsingular Implementation of the Mellor-Yamada Level 2.5 Scheme in the NCEP Meso model,
20 *Natl. Centers Environ. Predict.*, 61 [online] Available from:
21 <http://www.emc.ncep.noaa.gov/officenotes/newernotes/on437.pdf>, 2001.

22 Janjic, Z.: A nonhydrostatic model based on a new approach, *Meteorol. Atmos. Phys.*, 82, 271–285,
23 doi:10.1007/s00703-001-0587-6, 2003.

24 Janjic, Z.: A unified model approach from meso to global scales, in *EGU General Assembly Conference*
25 *Abstracts*, vol. 7, European Geosciences Union 2005., 2005.

26 Janjic, Z. and Black, T.: An ESMF unified model for a broad range of spatial and temporal scales, in *EGU*
27 *General Assembly Conference Abstracts*, vol. 9, European Geosciences Union 2007., 2007.

28 Janjic, Z. and Gall, R.: Scientific documentation of the NCEP nonhydrostatic multiscale model on the B grid
29 (NMMB). Part 1 Dynamics, , (April), 72, doi:10.5065/D6WH2MZX, 2012.

30 Janjic, Z., Gerrity, J. and Nickovic, S.: An Alternative Approach to Nonhydrostatic Modeling, Part III: Nonlinear
31 Mountain Wave Test, *World Meteorol. Organ. TD*, 5–15, 2000.

32 Janjic, Z., Huang, H. and Lu, S.: A unified atmospheric model suitable for studying transport of mineral aerosols
33 from meso to global scales, *IOP Conf. Ser. Earth Environ. Sci.*, 7, 12011, doi:10.1088/1755-1307/7/1/012011,
34 2009.

1 Janjic, Z., Janjic, T. and Vasic, R.: A Class of Conservative Fourth-Order Advection Schemes and Impact of
2 Enhanced Formal Accuracy on Extended-Range Forecasts, *Mon. Weather Rev.*, 139(1973), 1556–1568,
3 doi:10.1175/2010MWR3448.1, 2011.

4 Jay, J., Costa, F., Pritchard, M., Lara, L., Singer, B. and Herrin, J.: Erratum to “Locating magma reservoirs using
5 InSAR and petrology before and during the 2011-2012 Cordón Caulle silicic eruption,” *Earth Planet. Sci. Lett.*,
6 395, 254–266, doi:10.1016/j.epsl.2014.07.021, 2014.

7 Jöckel, P., von Kuhlmann, R., Lawrence, M. G., Steil, B., Brenninkmeijer, C. M., Crutzen, P. J., Rasch, P. J. and
8 Eaton, B.: On a fundamental problem in implementing flux-form advection schemes for tracer transport in 3-
9 dimensional general circulation and chemistry transport models, *Q. J. R. Meteorol. Soc.*, 127(September 2015),
10 1035–1052, doi:10.1002/qj.49712757318, 2001.

11 Jorba, O., Dabdub, D., Blaszcak-Boxe, C., Pérez, C., Janjic, Z., Baldasano, J. M., Spada, M., Badia, A. and
12 Gonçalves, M.: on global air quality with the NMMB/BSC chemical transport model, *J. Geophys. Res.*,
13 117(August), doi:10.1029/2012JD017730, 2012.

14 Kidder, S. and VonderHaar, T.: *Satellite meteorology: an introduction*, Academic Press, NY., 1995.

15 Lin, J. C.: Lagrangian Modeling of the Atmosphere: An Introduction, in *Lagrangian Modeling of the Atmosphere*,
16 pp. 1–11, American Geophysical Union., 2012.

17 Lorenz, E. N.: Energy and numerical weather prediction, *Tellus*, 12, 364–373, 1960.

18 Marti, A., Folch, A. and Jorba, O.: On-line coupling of volcanic ash and aerosols transport with multiscale
19 meteorological models, in *IAVCEI 2013 Scientific Assembly*, Kagoshima, Japan., 2013.

20 Marti, A., Folch, A. and Jorba, O.: On-line coupling of volcanic ash and aerosols transport with multi-scale
21 meteorological models, in *Cities on Volcanoes 8*, Jakarta, Indonesia., 2014.

22 Mastin, L. G., Guffanti, M., Servranckx, R., Webley, P., Barsotti, S., Dean, K., Durant, A., Ewert, J. W., Neri,
23 A., Rose, W., Schneider, D., Siebert, L., Stunder, B., Swanson, G., Tupper, A., Volentik, A. and Waythomas, C.
24 F.: A multidisciplinary effort to assign realistic source parameters to models of volcanic ash-cloud transport and
25 dispersion during eruptions, *J. Volcanol. Geotherm. Res.*, 186(1–2), 10–21,
26 doi:10.1016/j.jvolgeores.2009.01.008, 2009.

27 Mastin, L. G., Van Eaton, A. and Lowenstern, J.: Modeling ash fall distribution from a Yellowstone
28 supereruption, *Geochemistry, Geophys. Geosystems*, 15(8), 3459–3475, doi:10.1002/2014GC005469, 2014.

29 Mellor, G. L. and Yamada, T.: Development of a turbulence closure model for geophysical fluid problems, *Rev.*
30 *Geophys.*, 20(4), 851–875, doi:10.1029/RG020i004p00851, 1982.

31 Mesinger, F.: Forward-backward scheme, and its use in a limited area model., *Beitr. Phys. Atmos.*, 50, 200–210,
32 1977.

33 Mlawer, E., Taubman, S., Brown, P., Iacono, M. and Clough, S.: Radiative transfer for inhomogeneous
34 atmospheres: RRTM, a validated correlated-k model for the longwave, *J. Geophys. Res. Atmos.*, 102(D14),
35 16663–16682, doi:10.1029/97JD00237, 1997.

1 Monin, A. S. and Obukhov, A. M.: Basic laws of turbulent mixing in the surface layer of the atmosphere,
2 *Contrib. Geophys. Inst. Acad. Sci. USSR*, 24(151), 163–187, 1954.

3 Myhre, G., Shindell, D., Bréon, F. M., Collins, W., Fuglestedt, J., Huang, J., Koch, D., Lamarque, J.-F., Lee,
4 D., Mendoza, B., Nakajima, T., Robock, A., Stephens, G., Takemura, T. and Zhan, H.: 2013: Anthropogenic and
5 Natural Radiative Forcing, *Clim. Chang. 2013 Phys. Sci. Basis. Contrib. Work. Gr. I to Fifth Assess. Rep.*
6 *Intergov. Panel Clim. Chang.*, 659–740, doi:10.1017/CBO9781107415324.018, 2013.

7 Osores, M. S., Folch, A., Ruiz, J. and Collini, E.: Estimación de alturas de columna eruptiva a partir de imágenes
8 captadas por el sensor IMAGER del GOES-13, y su empleo para el pronóstico de dispersión y depósito de
9 cenizas volcánicas sobre Argentina, in *XIX Congreso Geológico Argentino.*, 2014.

10 Osores, M. S., Collini, E., Mingari, L., Folch, A., Ruiz, L., Toyos, G., Pujol, G., Farias, C., Alexander, P., Suaya,
11 M., Schonholz, T., Viramonte, J. G. and Villarosa, G.: Volcanic Ash Dispersion Modeling, Forecasting and
12 Remote Sensing in Argentina. Recent and future developments, in *IUGG - VW04 Remote Sensing and*
13 *Modelling of Volcanic Ash in Latin America*, International Union of Geodesy and Geophysics (IUGG), Czech
14 Republic., 2015.

15 Pérez, C., Hausteine, K., Janjic, Z., Jorba, O., Huneeus, N., Baldasano, J. M., Black, T., Basart, S., Nickovic, S.,
16 Miller, R. L., Perlwitz, J. P., Schulz, M. and Thomson, M. J.: Atmospheric dust modeling from meso to global
17 scales with the online NMMB/BSC-Dust model; Part 1: Model description, annual simulations and evaluation,
18 *Atmos. Chem. Phys.*, 11, 13001–13027, doi:10.5194/acp-11-13001-2011, 2011.

19 Pfeiffer, T., Costa, A. and Macedonio, G.: A model for the numerical simulation of tephra fall deposits, *J.*
20 *Volcanol. Geotherm. Res.*, 140, 273–294, doi:10.1016/j.jvolgeores.2004.09.001, 2005.

21 Pistolesi, M., Cioni, R., Bonadonna, C., Elissondo, M., Baumann, V., Bertagnini, A., Chiari, L. and Gonzales,
22 R.: Complex dynamics of small-moderate volcanic events: the example of the 2011 rhyolitic Cordón Caulle
23 eruption, Chile, *Bull. Volcanol.*, 77(3), doi:10.1007/s00445-014-0898-3, 2015.

24 Prata, A. J.: Infrared radiative transfer calculations for volcanic ash clouds, *Geophys. Res. Lett.*, 16(11), 1293–
25 1296, doi:10.1029/GL016i011p01293, 1989a.

26 Prata, A. J.: Observations of volcanic ash clouds in the 10–12 μm window using AVHRR/2 data, *Int. J. Remote*
27 *Sens.*, 10(4–5), 751–761, doi:10.1080/01431168908903916, 1989b.

28 Prata, A. J.: *Volcanic Information Derived from Satellite Data.*, 2011.

29 Pyle, D.: The thickness, volume and grainsize of tephra fall deposits, *Bull. Volcanol.*, 51(1), 1–15,
30 doi:10.1007/BF01086757, 1989.

31 Raga, G. B., Baumgardner, D., Ulke, a. G., Torres Brizuela, M. and Kucienska, B.: The environmental impact of
32 the Puyehue-Cordon Caulle 2011 volcanic eruption on Buenos Aires, *Nat. Hazards Earth Syst. Sci.*, 13, 2319–
33 2330, doi:10.5194/nhess-13-2319-2013, 2013.

34 Rood, R. B.: Numerical advection algorithms and their role in atmospheric transport and chemistry models, *Rev.*
35 *Geophys.*, 25(1), 71–100, doi:10.1029/RG025i001p00071, 1987.

1 Rose, W. and Durant, A.: Fine ash content of explosive eruptions, *J. Volcanol. Geotherm. Res.*, 186(1–2), 32–39,
2 doi:10.1016/j.jvolgeores.2009.01.010, 2009.

3 Schmid, R.: Descriptive nomenclature and classification of pyroclastic deposits and fragments, *Geol.*
4 *Rundschau*, 70(2), 794–799, doi:10.1007/BF01822152, 1981.

5 Scollo, S., Del Carlo, P. and Coltelli, M.: Tephra fallout of 2001 Etna flank eruption: Analysis of the deposit and
6 plume dispersion, *J. Volcanol. Geotherm. Res.*, 160(1–2), 147–164, doi:10.1016/j.jvolgeores.2006.09.007, 2007.

7 Scollo, S., Kahn, R. A., Nelson, D. L., Coltelli, M., Diner, D. J., Garay, M. J. and Realmuto, V. J.: MISR
8 observations of Etna volcanic plumes, *J. Geophys. Res. Atmos.*, 117(6), 1–13, doi:10.1029/2011JD016625,
9 2012.

10 Self, S.: The effects and consequences of very large explosive volcanic eruptions., *Philos. Trans. A. Math. Phys.*
11 *Eng. Sci.*, 364(June), 2073–2097, doi:10.1098/rsta.2006.1814, 2006.

12 Simmons, a. J. and Burridge, D. M.: An Energy and Angular-Momentum Conserving Vertical Finite-Difference
13 Scheme and Hybrid Vertical Coordinates, *Mon. Weather Rev.*, 109, 758–766, doi:10.1175/1520-0493, 1981.

14 Sommer, B.: Ash Cloud from Chilean volcano entering New Zealand Airspace, *Civ. Aviat. Auth. New Zeal.*
15 [online] Available from: https://www.caa.govt.nz/publicinfo/med_rel_Ash_Cloud.htm, 2011.

16 Spada, M., Jorba, O., Pérez, C., Janjic, Z. and Baldasano, J. M.: Modeling and evaluation of the global sea-salt
17 aerosol distribution: Sensitivity to emission schemes and resolution effects at coastal/orographic sites, *Atmos.*
18 *Chem. Phys.*, 13, 11735–11755, doi:10.5194/acp-13-11735-2013, 2013.

19 Sparks, R. S. J., Bursik, M., Carey, S., Gilbert, J., Glaze, L., Sigurdsson, H. and Woods, A.: *Volcanic Plumes*, 1
20 edition., John Wiley, Chichester, U.K., 1997.

21 Stuefer, M., Freitas, S. R., Grell, G., Webley, P., Peckham, S. and McKeen, S. a.: Inclusion of Ash and SO₂
22 emissions from volcanic eruptions in WRF-CHEM: development and some applications, *Geosci. Model Dev.*
23 *Discuss.*, 5, 2571–2597, doi:10.5194/gmdd-5-2571-2012, 2013.

24 Sulpizio, R., Folch, A., Costa, A., Scaini, C. and Dellino, P.: Hazard assessment of far-range volcanic ash
25 dispersal from a violent Strombolian eruption at Somma-Vesuvius volcano, Naples, Italy: Implications on civil
26 aviation, *Bull. Volcanol.*, 74(9), 2205–2218, doi:10.1007/s00445-012-0656-3, 2012.

27 Suzuki, T.: A theoretical model for dispersion of tephra, *Arc Volcanism Phys. Tectonics*, 93–113, 1983.

28 Suzuki, Y. and Koyaguchi, T.: A three-dimensional numerical simulation of spreading umbrella clouds, *J.*
29 *Geophys. Res.*, 114, 1–18, doi:10.1029/2007JB005369, 2009.

30 Vukovic, A., Rajkovic, B. and Janjic, Z.: Land Ice Sea Surface Model: Short Description and Verification, in
31 2010 International Congress on Environmental Modelling and Software Modelling for Environment's Sake,
32 Fifth Biennial Meeting, Ottawa, Canada, 5–8 July 2010., 2010.

33 Wessel, P. and Smith, W. H. F.: Free software helps map and display data, *Eos, Trans. Am. Geophys. Union*,
34 72(41), 441–441, doi:10.1029/90EO00319, 1991.

- 1 Wilson, L. and Huang, T. C.: The influence of shape on the atmospheric settling velocity of volcanic ash
2 particles, *Earth Planet. Sci. Lett.*, 44(2), 311–324, doi:10.1016/0012-821X(79)90179-1, 1979.
- 3 Wilson, T., Stewart, C., Bickerton, H., Baxter, P., Outes, V., Villarosa, G. and Rovere, E.: Impacts of the June
4 2011 Puyehue-Cordón Caulle volcanic complex eruption on urban infrastructure, agriculture and public health.
5 GNS Science Report., 2013.
- 6 Woodhouse, M., Hogg, a. J., Phillips, J. C. and Sparks, R. S. J.: Interaction between volcanic plumes and wind
7 during the 2010 Eyjafjallajökull eruption, Iceland, *J. Geophys. Res. Solid Earth*, 118, 92–109,
8 doi:10.1029/2012JB009592, 2013.
- 9 Zhang, L., Gong, S., Padro, J. and Barrie, L.: A size-segregated particle dry deposition scheme for an
10 atmospheric aerosol module, *Atmos. Environ.*, 35, 549–560, doi:10.1016/S1352-2310(00)00326-5, 2001.
- 11 Zhang, Y.: Online-coupled meteorology and chemistry models: history, current status, and outlook, *Atmos.*
12 *Chem. Phys.*, 8, 2895–2932, doi:10.5194/acp-8-2895-2008, 2008.
- 13 Zilitinkevich, S.: Bulk characteristics of turbulence in the atmospheric planetary boundary layer, *Tr. GGO*, 167,
14 49–52, 1965.
- 15

1

2 **Table 1. Main characteristics of the NMMB/BSC-ASH meteorological solver.**

<i>Meteorological Solver</i>	<i>Scheme</i>	<i>Reference</i>
Spatial discretization		
Multi-scale domain ranging from large eddy simulations (LES) to global simulations		Janjic (2005)
Conservativeness		
Conservation of mass, momentum, energy, enstrophy and a number of other first order and quadratic quantities. Positive definiteness and monotonicity are preserved by tracer advection		Janjic (1984)
Coordinates /Grid		
Horizontal coordinate	Rotated latitude-longitude for regional domains, and latitude-longitude coordinate with polar filter for global domains	Janjic et al. (2009); Janjic and Gall, (2012)
Vertical coordinate	Terrain following hybrid sigma-pressure	Simmons and Burridge, (1981)
Horizontal grid	Arakawa B-grid staggering	Janjic, 2005; Janjic and Black, 2007)
Vertical grid	Lorenz staggering	Lorenz, (1960)
Time integration schemes		
Horizontally propagating fast-waves	Forward-backward scheme	Ames, (1969); Gadd, (1974); Mesinger, (1977); Janjic, 1979)
Vertically propagating sound waves	Implicit scheme	Janjic and Gall, (2012)
Horizontal advection & Coriolis terms	Modified (Stable) Adams-Bashforth scheme	
Vertical advection	Crank-Nicolson scheme	Janjic, (1977,1984)
TKE generation and dissipation	Iterative	
Advection terms		
Horizontal	Energy and enstrophy conserving, quadratic conservative, second order	Janjic and Gall, (2012)
Vertical	Quadratic conservative, second order	Janjic and Gall, (2012)
Diffusion terms		
Vertical	Surface layer scheme	Janjic (1994, 1996)
Lateral	Smagorinsky non-linear approach	Janjic (1990)
Physics Options		
Microphysics/Clouds	Ferrier (Eta)	Ferrier et al. (2002)
Short and Longwave Radiation	Rapid Radiative Transfer Model (RRTM)	Mlawer et al. (1997); Pérez et al. (2011)
Surface Layer	NMMB similarity theory scheme: Based on Monin-Obukhov similarity theory with Zilitinkevich thermal roughness length	Monin and Obukhov (1954); (Zilitinkevich, 1965); Janjic (1994, 1996)
Land Surface, Heat & moisture surface flux	LISS model	Vukovic et al. (2010)
Planetary Boundary layer / free atmosphere	Mellor-Yamada-Janjic scheme	Mellor and Yamada, (1982); Janjic (1996, 2001)
Convective adjustments	Betts-Miller-Janjic scheme	Betts and Miller, (1986); Janjic (1994, 2000).

Alex Marti 20/1/2017 16:52

Deleted: Nicholson

3

4

1 **Table 2. Options implemented in NMMB/BSC-ASH to estimate the mass eruption rate from column height. Unless**
 2 **otherwise noted, the units for all parameters are in SI.**

Reference	MER schemes	Eq.	Parameters
Mastin et al., (2009)	$MER = \bar{\rho} \left[\frac{0.5 H_{plume}}{10^3} \right]^{0.241}$	(1)	$\bar{\rho}$ = magma density (2500 kg m ⁻³) H_{plume} = column height above the vent (m)
Degruyter and Bonadonna (2012)	$MER = \pi \frac{\rho_{a0}}{g'} \left(\frac{\alpha^2 \bar{N}^3}{z_1^4 n} H_{plume}^4 + \frac{\beta^2 \bar{N}^2 \bar{v}}{6} H_{plume}^3 \right)$ $g' = g \left(\frac{c_0 \theta_0 - c_{a0} \theta_{a0}}{c_{a0} \theta_{a0}} \right)$	(2)	ρ_{a0} = atmospheric density at the vent (kg m ⁻³) g' = reduced gravity \bar{N} = average buoyancy frequency (s ⁻¹) \bar{v} = average wind velocity across column height (m s ⁻¹) z_1 = Max. non-dimensional height α, β = radial and crossflow entrainment coefficients g = gravitational acceleration (9.81 m s ⁻²) c_0 = source specific heat capacity (J kg ⁻¹ K ⁻¹) c_{a0} = specific heat capacity of the atmosphere (J kg ⁻¹ K ⁻¹) θ_0 = source temperature (K) θ_{a0} = atmospheric temperature (K)
Woodhouse et al. (2013)	$MER = 0.35 \alpha^2 f(W_s)^4 \frac{\rho_{a0}}{g'} N^3 H_{plume}^4$ $f(W_s) = \frac{1.44 \dot{\gamma}}{\bar{N}}$ $g' = g \left(\frac{c_s n_0 + c_s (1 - n_0) \theta_0 - c_a \theta_{a0}}{c_a \theta_{a0}} \right)$	(3)	Q = mass flux (kg s ⁻¹) W_s = dimensionless wind strength \bar{N} = average buoyancy frequency (s ⁻¹) $\dot{\gamma}$ = shear rate of atmospheric wind (s ⁻¹) c_s = specific heat of solids (J kg ⁻¹ K ⁻¹) c_a, c_s = specific heat of dry air (J kg ⁻¹ K ⁻¹) c_s = specific heat of water vapor (J kg ⁻¹ K ⁻¹)

Alex Marti 27/1/2017 14:48
 Formatted Table

Alex Marti 31/1/2017 13:24
 Formatted: Indent: Left: -3.37 cm

Alex Marti 27/1/2017 14:48
 Formatted: Font:7 pt

Alex Marti 31/1/2017 13:24
 Deleted: constant

3
 4 **Table 3. Ash aggregation options in NMMB/BSC-ASH from analytical solutions based from field observations.**
 5 **Default aggregate properties can be modified by the user.**

Name	New aggregate class	Default properties	Reference
NONE	No aggregation processes	n/a	n/a
CORNELL	50% of the 63–44 μm class aggregate 75% of the 44–31 μm class aggregate 100% of the < 31 μm class aggregate	Diameter = 250 μm Density = 350 kg m ⁻³ Sphericity = 0.9	Based on Cornell et al. (1983) Campanian Ignimbrite's deposit (Y5 ash layer)
PERCENTAGE	Takes a user-defined fixed percentage from each particle class	Diameter = 250 μm Density = 350 kg m ⁻³	Based on Sulpizio et al. (2012)

6
 7 **Table 4. Governing equations for NMMB/BSC-ASH wet aggregation model.**

Wet aggregation scheme	Eq.	Parameters
Number of particles of a class aggregated per unit volume $\Delta n_j \approx \frac{\Delta n_{tot} N_j}{\sum_k N_k} \quad (k = k_{min}, \dots, k_{max})$	(5)	Δn_{tot} = number of particles that aggregate per time interval N_j = number of particles of diameter j in an aggregate k = aggregation class N_k = number of particles of diameter k in an aggregate

Number of particles aggregated during Δt	$N_j = k_f \left(\frac{d_A}{d_j} \right)^{D_f} \quad (6)$	k_f = fractal prefactor ≈ 1 D_f = fractal exponent ≤ 3 d_A = aggregate diameter d_j = primary particle diameter
Total particle decay per unit volume during Δt	$\Delta n_{tot} = \alpha_m \left((A_B n_{tot}^2 + A_S \phi^{3/D_f} n_{tot}^{2-3/D_f} + A_{DS} \phi^{4/D_f} n_{tot}^{2-4/D_f}) \right) \Delta t \quad (7)$	α_m = mean sticky efficiency ϕ = solid volume fraction
Number of particles available to aggregate	$n_{tot} = \sum_j \frac{6C_j}{\pi \rho_j d_j^3} \quad (8)$	n_{tot} = number of particles available to aggregate k_b = Boltzmann constant $1.38 \times 10^{-23} \text{ m}^2 \text{ kg s}^{-2} \text{ K}$ T = absolute temperature μ_o = dynamic viscosity of air Γ_s = fluid shear ξ = particle diameter to volume fractal relationship
Kernels	For Brownian motion: $A_B = -\frac{4k_b T}{3\mu_o}$ Ambient fluid shear: $A_S = \frac{2\Gamma_s \xi^4}{3}$ Differential sedimentation: $A_{DS} = -\frac{\pi(\rho_m - \rho_a)g\xi^4}{48\mu_o}$	ρ_m = mean particle density ρ_a = air density

1

2 **Table 5. Governing equations for NMMB/BSC-ASH gravity current model .**

Gravity current scheme	Eq.	Parameters
Effective radial velocity of the umbrella spreading	$u_b(t) = \frac{2}{3} \left(\frac{3\lambda N q}{2\pi} \right)^{1/3} t^{1/3} \quad (9)$ $u_b(R) = \left(\frac{2\lambda N q}{3\pi} \right)^{1/2} \frac{1}{\sqrt{R}}$	u_b = effective radial velocity as a function of time (t) or cloud radius (R) λ = empirical constant ($\lambda \approx 0.2$) (Suzuki and Koyaguchi, 2009) N = Brunt-Väisälä frequency (atm. ambient stratification) q = volumetric flow rate into the umbrella region
Volumetric flow rate into the umbrella region	$q = C \sqrt{k} \frac{M^{3/4}}{N^{5/8}} \quad (10)$ $C \begin{cases} 0.5 \times 10^4 \text{ m}^3 \text{ kg}^{-3/4} \text{ s}^{-7/8} \\ 1.0 \times 10^4 \text{ m}^3 \text{ kg}^{-3/4} \text{ s}^{-7/8} \end{cases}$	M = efficiency of air entrainment k = mass eruption rate C = location base constant C_A : for tropical eruptions C_B : for midlatitude and polar eruptions
Contribution of the gravitational spreading	$ct = \left(\frac{u_b}{u_b + u_w} \right) \times 100 \quad (11)$	u_w = wind field velocity
Radial distance (gravity vs. passive transport)	$Ri = \frac{u_b^2}{u_w^2} = \frac{4}{9} \left(\frac{3\lambda N q}{2\pi} \right)^{2/3} t^{-2/3} \quad (12)$	Ri = Richardson number $Ri > 1$: gravity-driven regime $Ri < 0.25$: passive transport regime

3

4 **Table 6. Settling velocity models in NMMB/BSC-ASH.**

NAME/Reference	Drag coefficient	Eq.	Description/ Parameters
ARASTOPOUR (Arastoopour et al., 1982)	$C_d = \begin{cases} \frac{24}{Re} \{1 + 0.15 Re^{0.687}\} & Re \leq 988.947 \\ 0.44 & Re > 988.947 \end{cases}$	(14)	For spherical particles only

GANSER (Ganser, 1993)	$C_d = \frac{24}{ReK_1} \{1 + 0.1118[Re(K_1K_2)]^{0.6567}\} + \frac{0.4305K_2}{1 + \frac{3305}{ReK_1K_2}} \quad (15)$ $K_1 = \frac{3}{[(d_n/d)]_{+2\psi^{-0.5}}}; K_2 = 10^{1.8148(-\text{Log}\psi)^{0.5743}}$ $\psi_{\text{work}} = 12.8 \frac{(P^2Q)^{1/3}}{1 + P(1+Q) + 6\sqrt{1 + P^2(1+Q^2)}}$	<p>For spherical and non-spherical particles</p> <p>K_1, K_2 = shape factors d_n = average between the min and max. axis d = sphere volume ψ_{work} = particle sphericity ($\psi=1$ for spheres)</p>
WILSON (Pfeiffer et al., 2005; Wilson and Huang, 1979)	$C_d = \begin{cases} \frac{24}{Re} \varphi^{-0.828} + 2\sqrt{1.07 - \varphi} & Re \leq 10^2 \\ 1 - \frac{C_d _{Re=10^2}}{900} (10^3 - Re) & 10^2 \leq Re \leq 10^3 \\ 1 & Re \leq 10^3 \end{cases} \quad (16)$	<p>ψ = particle aspect ratio $\psi = (b+c)2a^{-1}$ a, b, c = particle semi-axes</p>
DELLINO (Dellino et al., 2005)	$v_s = 1.2605 \frac{v_a}{d} (Ar\varepsilon^{1.6})^{0.5206} \quad (17)$ $Ar = g d^3 (\rho_p - \rho_a) \rho_a / \mu_a^2$	<p>For larger particles only</p> <p>Ar = Archimedes number g = gravity acceleration ε = particle shape factor μ_a = dynamic viscosity d = particle equivalent diameter, ρ_p = particle density ρ_a = air density</p>

1
2
3
4

Table 7. Model configuration for the 2011 Cordón Cauile regional and global runs. The regional run used a horizontal resolution of 0.15° x 0.15° with a 30s dynamic time-step, while the global domain used a horizontal resolution of 1° x 0.75° with a 180s dynamic time-step.

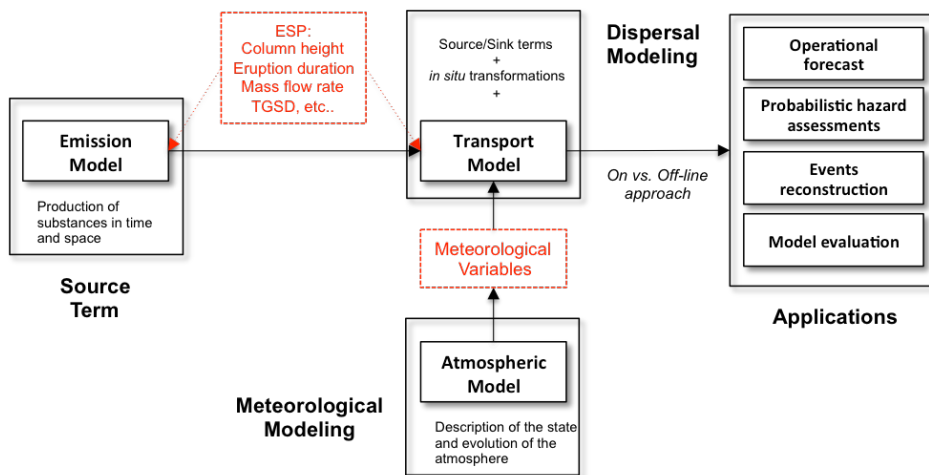
MODEL CONFIGURATION	
Dynamics	NMMB (30s/180s time-step)
Physics	Ferrier microphysics BMJ cumulus scheme MYJ PBL scheme LISS land surface model
Aerosols	11 ash bins (30s/180s time-step)
Source Term (emissions)	
Duration	20 days
Vertical distribution	Suzuki distribution
MER formulation	Mastin et al. (2009)
Aggregation model	Percentage
Sedimentation model	Ganser (1993)
Run Set-up	
Number of processors	512
Domain	Regional/Global
Horizontal resolution	0.15° x 0.15° / 1° x 0.75°
Vertical layers	60
Top of the atmosphere	21 hPa
Meteorology Boundary conditions (spatial resolutions)	ECMWF EraInterim Reanalysis (0.75° x 0.75°)

1

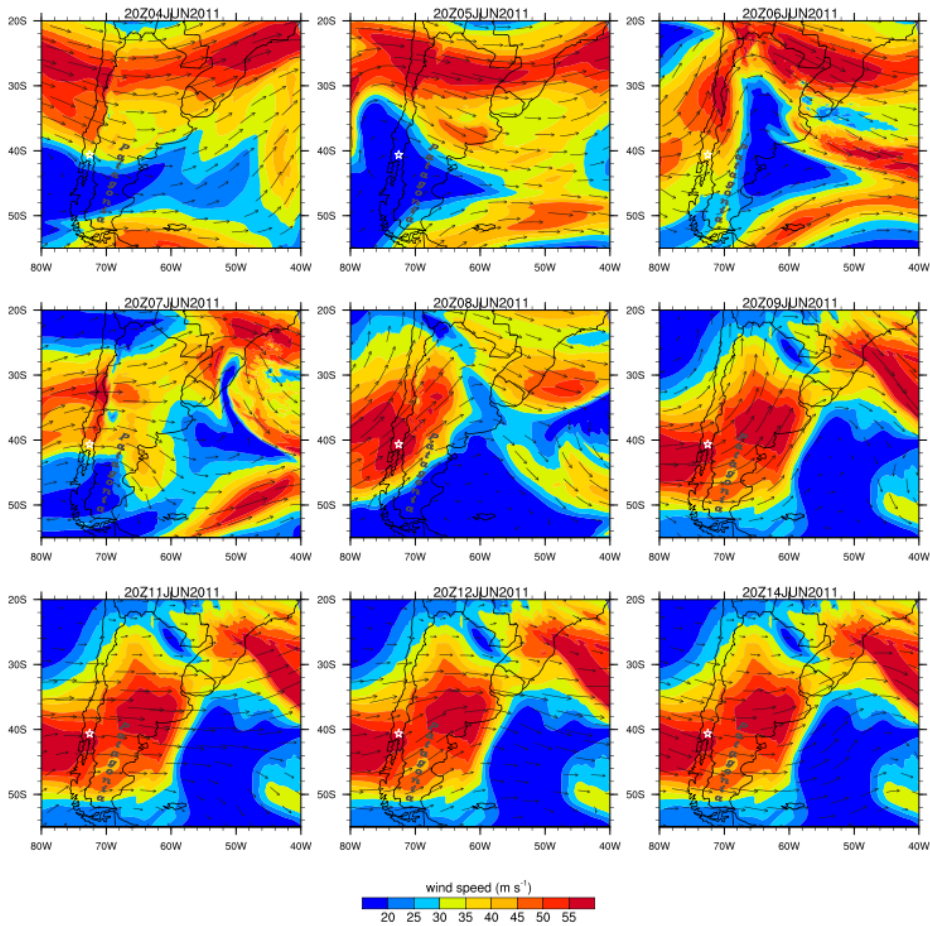
2 **Table 8. Model configuration for the 2001 Mt. Etna regional simulations. Regional Run1 used a horizontal resolution**
3 **of 0.1° x 0.1° with a 30s dynamic time-step, while Run2 used a finer horizontal resolution of 0.05° x 0.05° with a 10s**
4 **dynamic time-step.**

Source Term (emissions)	
Duration	3 days
Vertical distribution	Suzuki distribution
MER formulation	Mastin
Column height above the vent	2570
Ash bins	8
Aggregation model	
Cornell et al. (1983)	
Sedimentation model	
Ganser (1993)	
Run Set-up	
Number of processors	256
Domain	Regional 1 / Regional 2
Horizontal resolution	0.1° x 0.1° / 0.05° x 0.05°
Vertical layers	60
Top of the atmosphere	21 hPa
Meteorology Boundary conditions (spatial resolutions)	ECMWF ERA-Interim Reanalysis (0.75° x 0.75°)

5

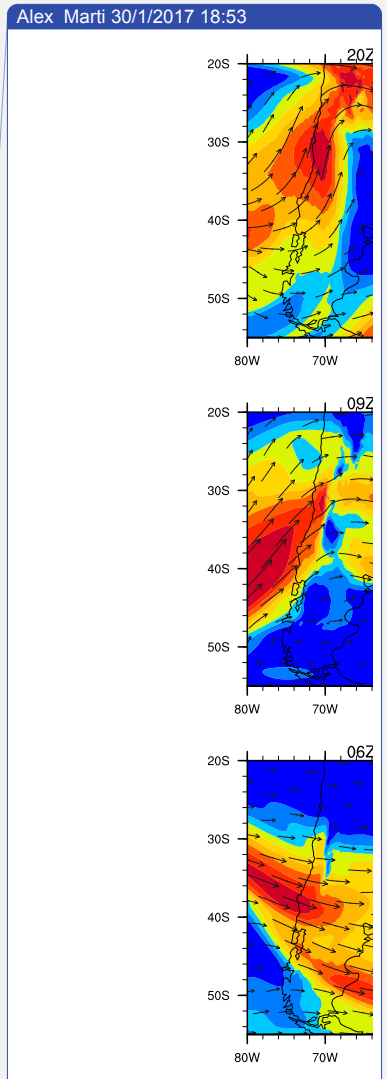


6 **Figure 1. Schematic representation of the main components of an Atmospheric Transport Model. Red text shows**
7 **model specifications for the transport of volcanic ash.**
8



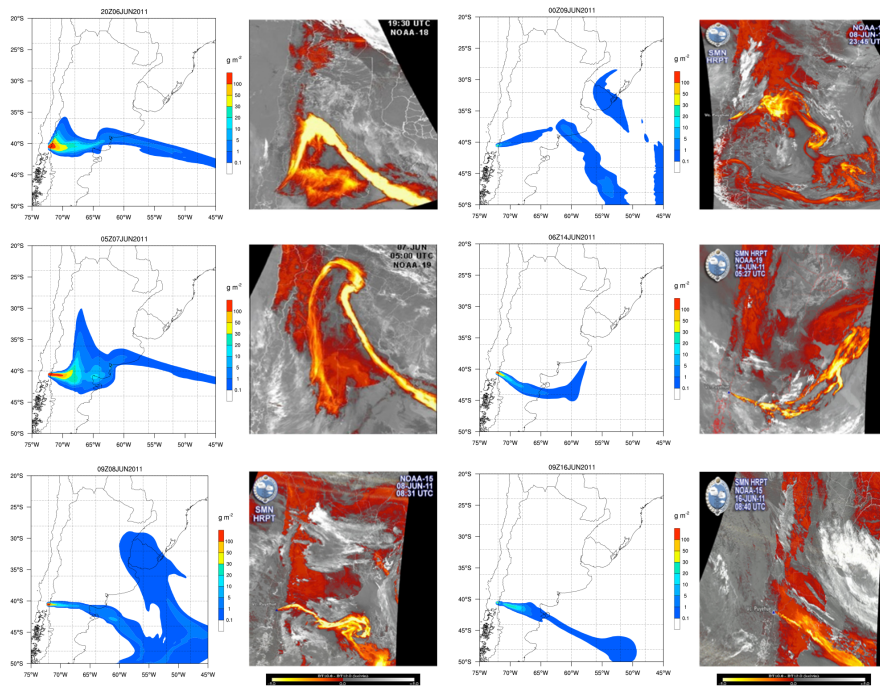
1
2
3
4
5

Figure 2. Meteorological synoptic situation during the first two weeks (4-14 June) of the 2011 Caulle (star) activity over South America. Plots show the direction (vector) and velocity (contours $m s^{-1}$) of the wind at 9100 m above ground level (300 hPa circa). Meteorological data obtained from the NMMB meteorological forecast driven with ERA-Interim reanalysis at 0.75° horizontal resolution.



Deleted:
Unknown
Formatted: Font color: Auto
Unknown
Formatted: Font:Bold, Font color: Auto
Alex Marti 27/1/2017 17:14
Deleted: Europe
Alex Marti 30/1/2017 18:48
Deleted: during 6-16 June.

1



2

3 **Figure 3.** Composite image of NMMB/BSC-ASH results for dispersion of ash for the 2011 Caule eruption at different
 4 time slices. Simulation results are compared against split windows algorithm NOAA-AVHRR satellite images ([bands](#)
 5 [11-12 microns](#)). Contours indicate ash column load (g m^{-2}) resulting from integrating the mass of the ash cloud along
 6 the atmospheric vertical levels.

7

Alex Marti 30/1/2017 18:53

Formatted: Don't keep with next

Unknown

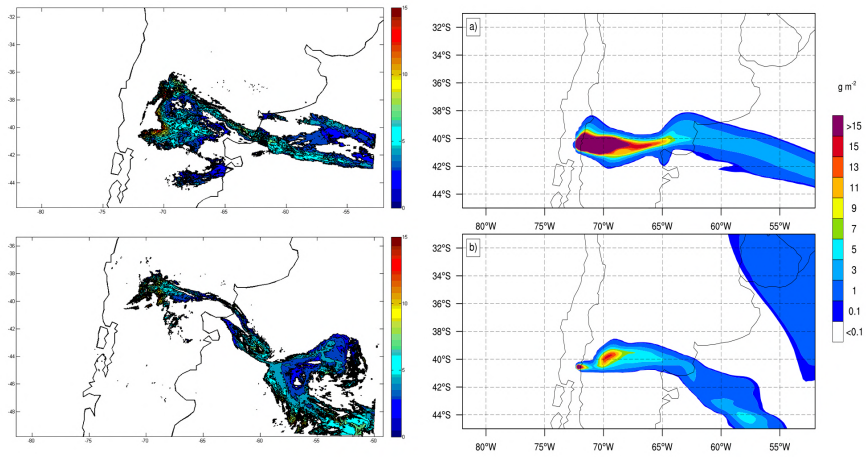
Formatted: Font color: Auto

Alex Marti 30/1/2017 18:53

Deleted: ... [2]

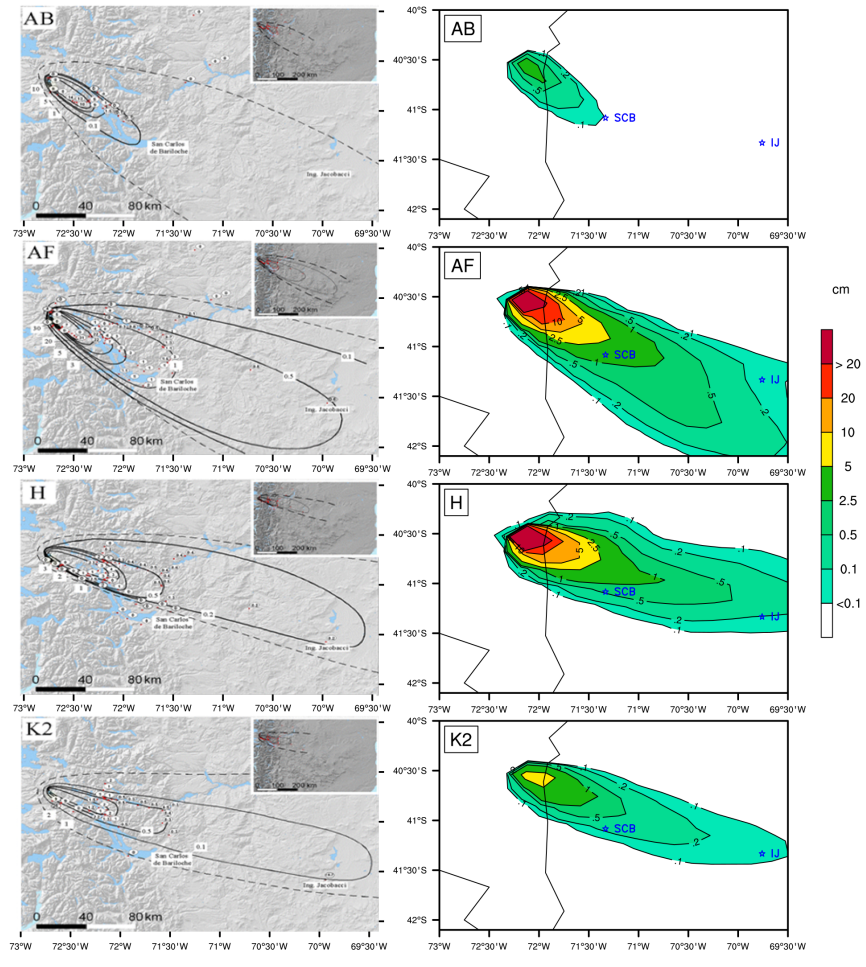
Unknown

Formatted: Font:Bold, Font color: Auto



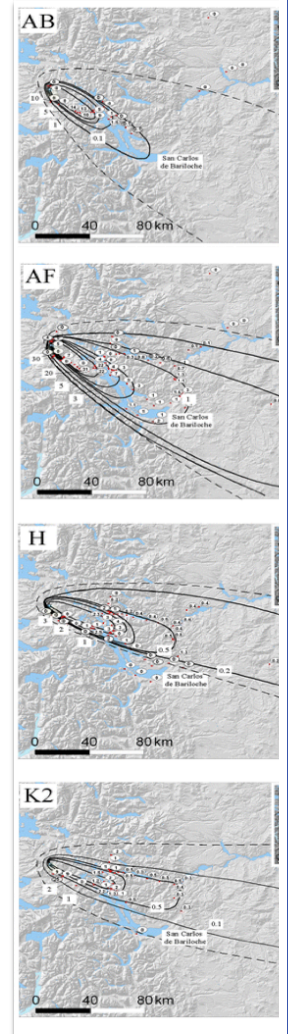
1
 2 | Figure 4. Left: Mass loadings (g m^{-2}) of the 2011 Caule volcanic ash cloud from the MODIS-based retrievals (Osoreo
 3 et al., 2015). Right: Predicted column mass (g m^{-2}) with NMMB/BSC-ASH for a) 6 June at 14:25 UTC and, b) 8 June
 4 at 14:15 UTC.

5

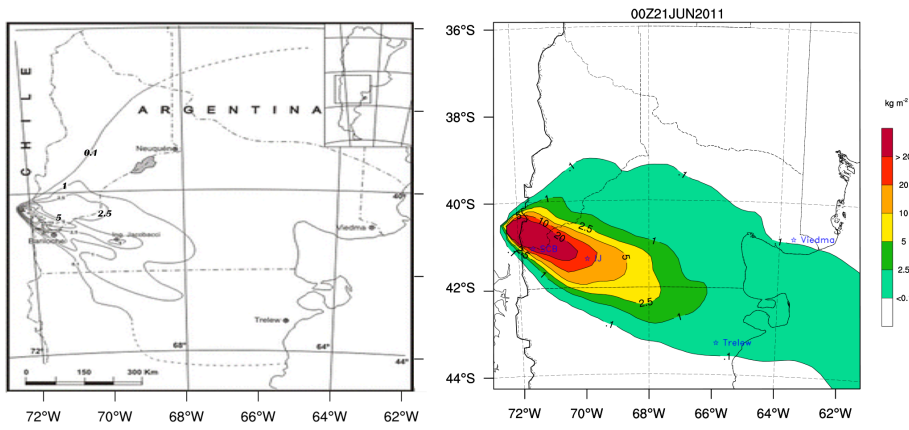


1
2
3
4
5

Figure 5. Left: Isopach maps in centimeter of layers A-B, A-F, H, and K2. Dashed lines infer the limit of the deposits presented in Pistolesi et al. (2015b). Right: Corresponding NMMB/BSC-ASH computed thicknesses (cm). Key locations in blue include San Carlos de Bariloche (SCB) and Ingeniero Jacobacci (IJ), 90 and 240 km east of the vent



Deleted:

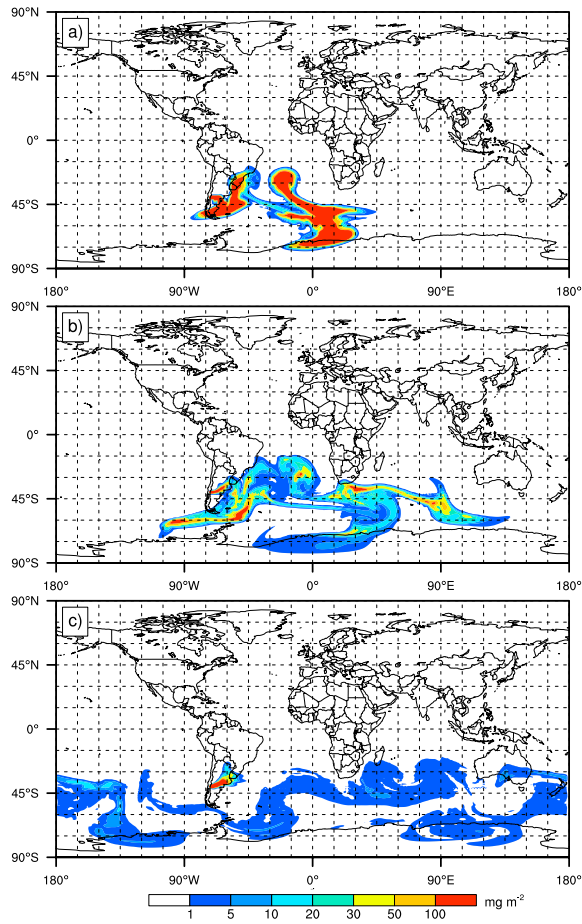


1
2
3
4
5
6
7

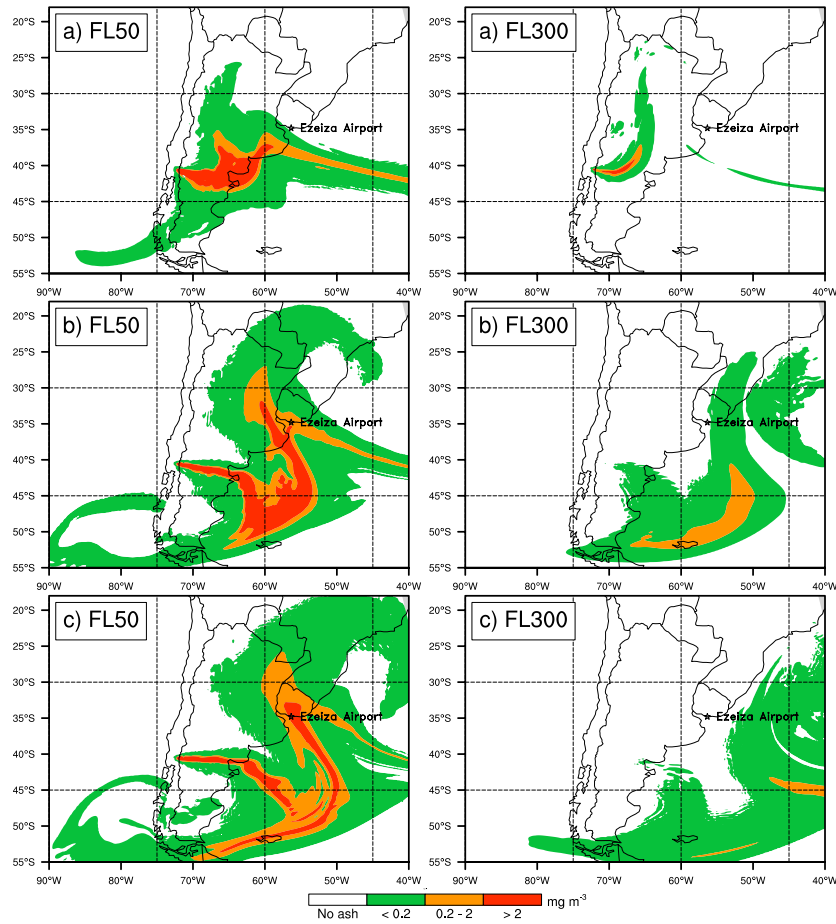
Figure 6. Left: measured ground deposit isopachs (kg m^{-2}) for the period beginning on 4 June until 30 June. Dashed lines infer the limit of the deposits (modified from Collini et al., 2013). Right: Predicted deposit load (kg m^{-2}) with NMMB/BSC-ASH at the end of the simulation. Key locations in blue include San Carlos de Bariloche (SCB; 90 km from the vent), Ingeniero Jacobacci (IJ; 240 km east of the vent), and Trelew and Viedma (~ 600 km SE and NE of the vent, respectively).

Unknown
Formatted: Font color: Auto
Alex Marti 31/1/2017 12:45

Deleted:
Unknown
Formatted: Font:Bold, Font color: Auto
Alex Marti 31/1/2017 12:46
Deleted: (



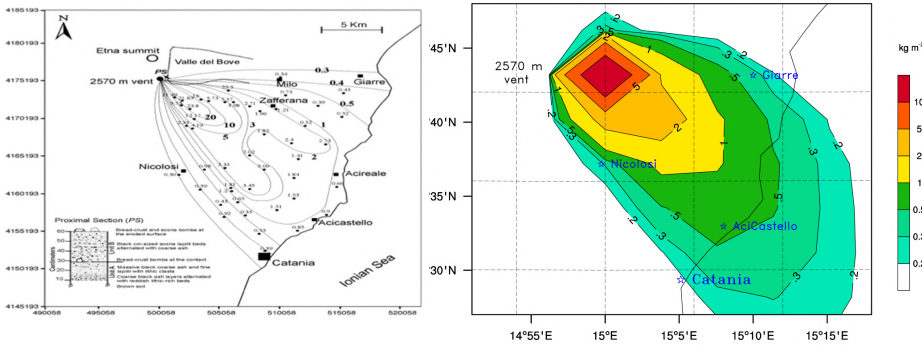
1
 2 **Figure 7. NMMB/BSC-ASH total column concentration (mass loading; mg m^{-3}) from our global simulation. Results**
 3 **for a) 8 June at 09:00 UTC, b) 10 June at 04:00 UTC, and c) 14 June at 06:00 UTC.**



1

2 **Figure 8. NMMB/BSC-ASH Flight level ash concentrations (mass loading; mg m^{-3}) before and after closure of the**
 3 **Buenos Aires (Ezeiza) airport and air space. Results for FL50 (left) and FL300 (right) for a) 6 June at 11:00 UTC, b) 7**
 4 **June at 04:00 UTC, and c) 7 June at 12:00 UTC. Safe ash concentration thresholds are shown (red contours illustrate**
 5 **"No Flying" zones).**

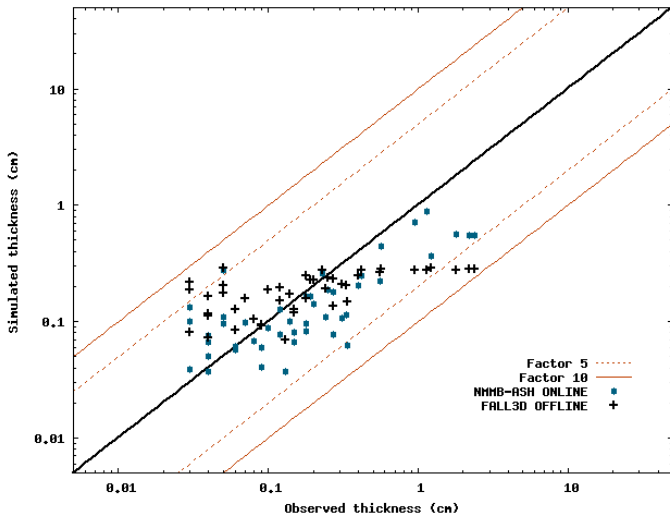
6



1
 2 Figure 9. Left: Isomass map of the tephra deposit formed between 21 and 24 July 2001. Curves are given in kg m^{-2} .
 3 | Coordinates are given in UTM-Datum ED50 (Scollo et al., 2007). Right: Modeled deposit load (kg m^{-2}) with
 4 NMMB/BSC-ASH at the end of the event.

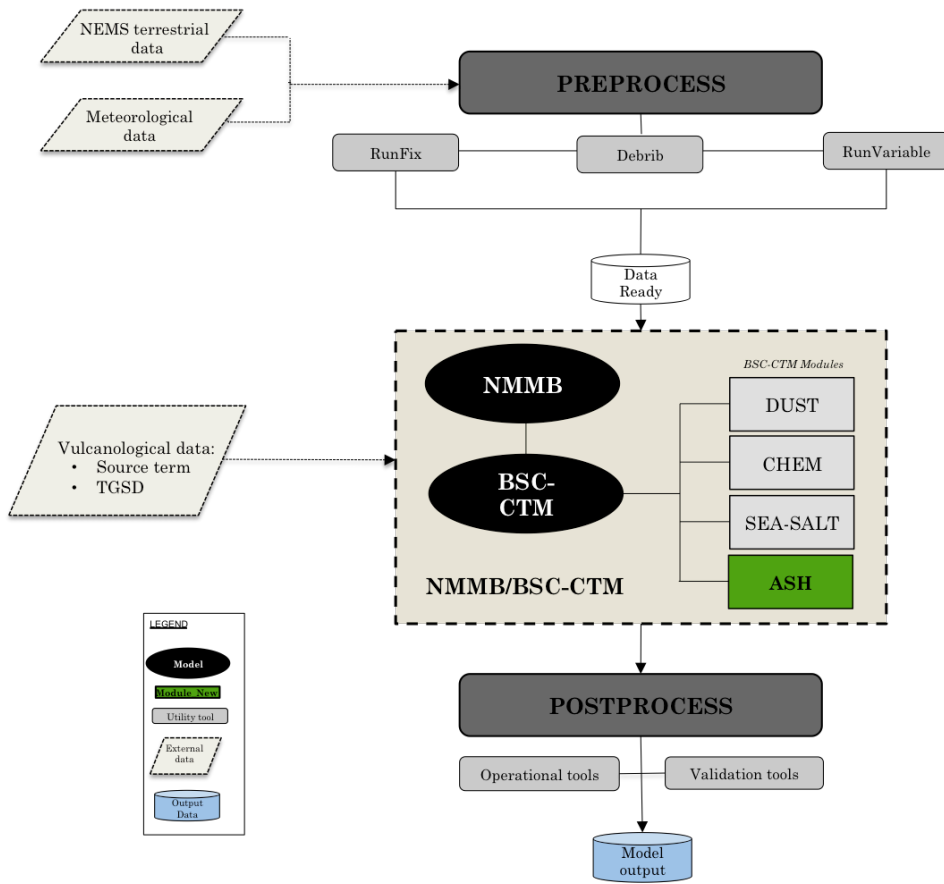
Alex Marti 27/1/2017 17:10
 Deleted: Predicted

5

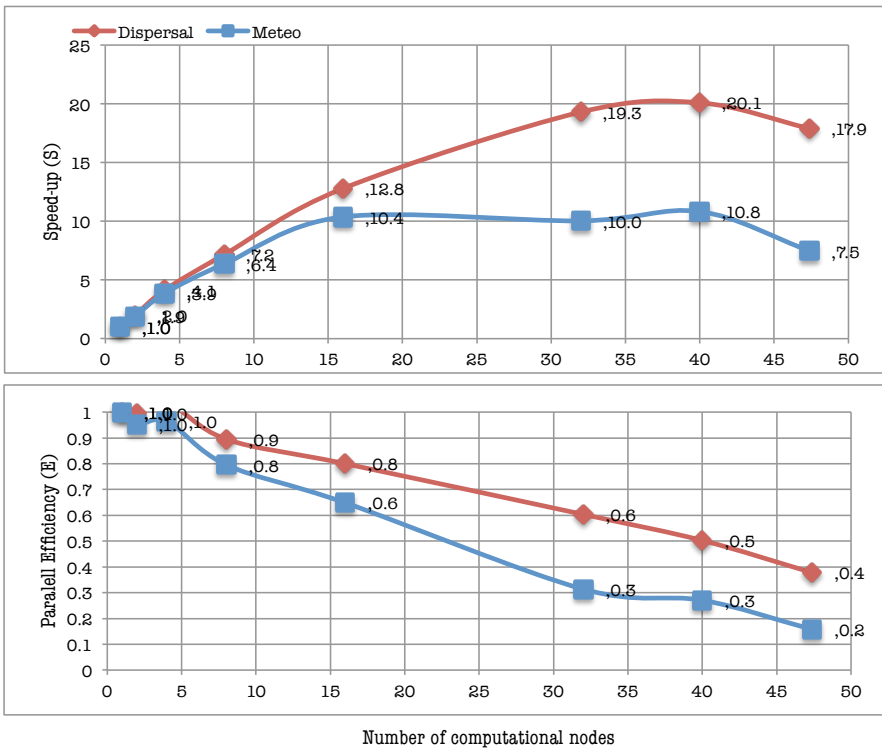


6
 7 Figure 10. Simulated versus observed thicknesses for the reconstruction of the 2011 Etna eruption with NMMB-ASH
 8 (circles) and FALL3D (crosses). The solid bold line represents a perfect agreement, while the dashed and solid thin
 9 orange lines mark the region that is different from observed thicknesses by a factor 5 (1/5) and 10 (1/10), respectively

10

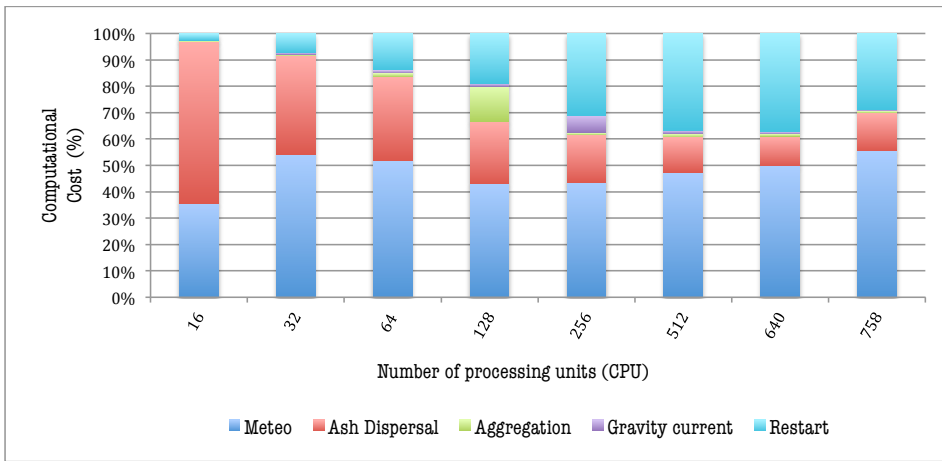


1
 2 **Figure 11. Schematic representation of the operational implementation of NMMB/BSC-ASH.**
 3



1
2
3
4
5
6

Figure 12. Figure NMMB/BSC-ASH scalability results. Top: parallel speed-up (S; computational speed) for meteorology only (blue) and for meteorology and dispersal combined (red). Bottom: parallel efficiency (E) versus number of computation nodes employed.



1
2
3
4

Figure 13. NMMB/BSC-ASH relative computational cost (%) with increasing CPUs. Represented processes include: Meteorology (blue); Ash dispersal for 10 bins (red); Aggregation (green); Gravity current (purple) and; Restart (light blue).